Bioorganic Chemistry 93 (2019) 103317

Contents lists available at ScienceDirect

Bioorganic Chemistry

journal homepage: www.elsevier.com/locate/bioorg

Design and synthesis of substituted dihydropyrimidinone derivatives as cytotoxic and tubulin polymerization inhibitors

Sravani Sana[a], Ramya Tokala[a], Deepti Madanlal Bajaj[b], Narayana Nagesh[d], Kiran Kumar Bokara[d], Gaddam Kiranmai[d], Uppu Jaya Lakshmi[a], Swapna Vadlamani[c], Venu Talla[b], Nagula Shankaraiah[a,*]

[a] Department of Medicinal Chemistry, National Institute of Pharmaceutical Education and Research (NIPER), Hyderabad 500 037, India
[b] Department of Pharmacology and Toxicology, National Institute of Pharmaceutical Education and Research (NIPER), Hyderabad 500 037, India
[c] Department of Pharmaceutical Technology in Process Chemistry, National Institute of Pharmaceutical Education and Research (NIPER), Hyderabad 500 037, India
[d] CSIR-Centre for Cellular and Molecular Biology, Medical Biotechnology Complex, ANNEXE II, Uppal Road, Uppal, Hyderabad 500007, India

ARTICLE INFO

Keywords:
Tubulin polymerization
Biginelli reaction
α-bromoacrylamide dihydropyrimidinones
Cytotoxicity
Apoptosis

ABSTRACT

An operationally simple Biginelli protocol was employed for the synthesis of new C6-carbon based aryl α-haloacrylamide-linked dihydropyrimidinone derivatives. The synthesized compounds were appraised for their *in vitro* antiproliferative potential against a selected panel of human cancer cell lines especially MCF-7 (human breast cancer), MDA-MB-231 (human breast cancer), HCT-116 (human colon cancer), HCT-15 (human colorectal adenocarcinoma), HT-29 (human colon adenocarcinoma) and DU145 (human prostate cancer) along with normal lung fibroblasts (HFL-1). Preferably, compounds containing α-haloacrylamide (**10a-g**) functionality were found to exhibit most significant cytotoxicity (IC_{50} value 0.54 ± 0.12 to 8.35 ± 0.82 μM) against the listed cancer cell lines, particularly towards breast cancer cell lines MCF-7 and MDA-MB-231 (IC_{50} value 0.54 ± 0.12 to 3.70 ± 0.24 μM). In the seam of synthesized compounds, compound **10f** exhibited potent antiproliferative activity against breast cancer cell lines namely MCF-7 (IC_{50} value 0.54 ± 0.12 μM) and MDA-MB-231 (IC_{50} value 1.18 ± 0.32 μM). Further to understand the underlying apoptosis mechanisms, different staining techniques such as AO/EB, DCFDA, and DAPI staining were performed. To know the extent of apoptosis and loss of mitochondrial membrane potential in MCF-7 cell lines, annexin V-FITC/PI and JC-1 were performed. Cell cycle analysis revealed that compound **10f** arrested the cells at G2/M phase in a dose-dependent manner. The compound **10f** also found to exhibit significant inhibition of tubulin polymerization (IC_{50} of 6.91 ± 0.43 μM) with microtubule destabilizing properties. Molecular docking studies also revealed that compound **10f** efficiently interacted with critical catalytically active residues Ser178, Val238, and Val318 of the α/β-tubulin by a hydrogen bond.

1. Introduction

Cancer is a pernicious disease connecting to a bundle of cellular processes, in which a group of cells become abnormal, remarked as a major public health problem worldwide [1]. Universal cancer epidemic is set to promote and estimated 12 million deaths per year by 2030 [2]. Despite the heroic developments, cancer still remained as a focus of interest due to the emergence of multi-drug resistance, toxicity and clearly drives the need for the development of new anticancer agents for better clinical benefits [3].

Microtubule is the cage of tubulin dimers, involves in the dynamics of chromosomes specifically, mitotic spindle formation during cell division and placed as an important target for anticancer therapy [4]. A large number of natural as well as semi-synthetic derivatives [5] have been found to inhibit tubulin polymerization. Nonetheless, no ideal member of this class has been succeeded clinically because of toxicity, flat water solubility leading to poor patient compliance and multi-drug resistance [6]. Therefore, it created an urgent need to develop novel tubulin inhibitors, hoping to find a way to solve the unsolved problems to date and to come-up with new binding sites of tubulin expanding the scope for future cancer treatment [7].

Pyrimidine acts as a potential framework for DNA and RNA, elucidating its importance in drug discovery and development [8]. Small molecule inhibitors containing dihydropyrimidinone as a core have

* Corresponding author.
E-mail address: shankar@niperhyd.ac.in (N. Shankaraiah).

https://doi.org/10.1016/j.bioorg.2019.103317
Received 16 May 2019; Received in revised form 17 September 2019; Accepted 26 September 2019
Available online 26 September 2019

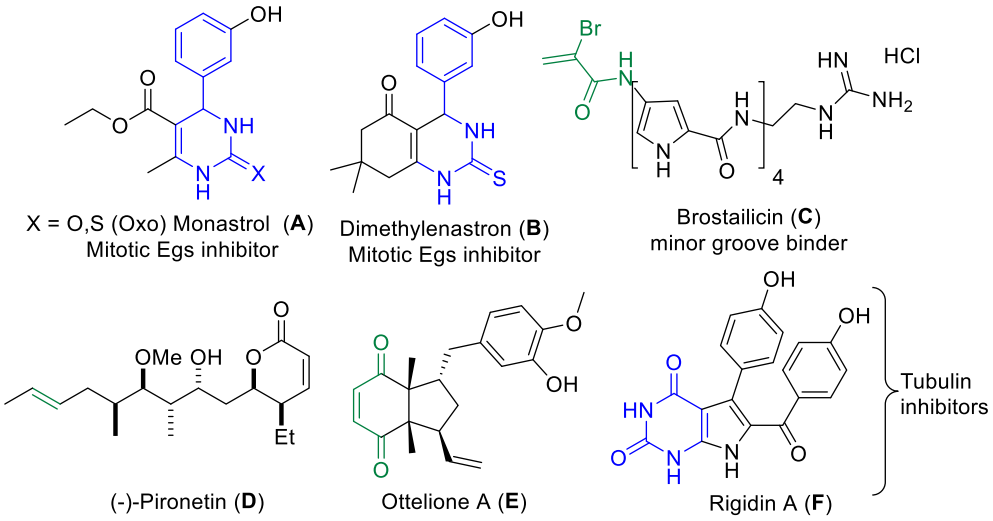

Fig. 1. Structures of minor groove binder, mitotic Egs and tubulin inhibitors.

been observed to possess distinct pharmacological activities such as anticancer (**B** and **F**, Fig. 1) [9], antihypertensive [10], analgesic [11], antimicrobial [12], anti-inflammatory [13], antitubercular [14], anti-HIV, A2B adenosine receptor antagonists and antibacterial activity [15]. Besides, dihydropyrimidinone was found to exert their cytotoxicity through varied mechanisms, includes inhibition of Eg5 kinesin [16], α-amino-β-carboxymuconate-ε-semi aldehyde decarboxylase [17], and tubulin polymerization. Monastrol (**A**, Fig. 1) is the first dihydropyrimidinone based small molecule identified as an inhibitor of mitotic spindle protein, Eg5 that helps in spindle formation during mitosis [18]. Continually, CYT-997, a highly cytotoxic pyrimidine derivative was identified against a range of cancer cell lines through microtubule destabilization and also acts as vascular disrupting agent [19].

In addition, the diversely targeted covalent strategy has widened the drug discovery since the 1990s with clear insights of hetero Michael addition reaction with thiols of a cys-residue of a particular protein, expands the ligand binding affinity and selectivity towards specific proteins [20]. α-Haloacryloyl is one such functional group animated from cytotoxic natural products like brostallicin (**C**, Fig. 1) [21], verongiaquinol, bromovulone, punaglandins and discorhabdin C, alkylates DNA through a reactive electrophile generated by thiol interaction [22]. Besides, pironetin (**D**, Fig. 1) [23] is a naturally derived α/β unsaturated lactone known till date as cell cycle inhibitor at M-phase by covalently binding to cysteine-316 of α-tubulin. Ottelione A (**E**, Fig. 1) is the naturally derived, most cytotoxic of sulfhydryl reactive drugs, also inhibits colchicine binding to tubulin [24]. Some of the other earlier examples, such as 2,4-dichloro benzyl thiocyanate interact covalently with tubulin at multiple cysteine residues, T138067 is also found to interact with β-tubulin, especially with cysteine-241 thiol group. Colchicine analogues with chloro acetyl groups attached to A-ring alkylates both cys-239 and cys-354 of β-tubulin [25].

Next, the rapid association of molecular diversity is an important achievement in modern drug discovery where addressing the challenges like intrinsic atom economy, time and energy savings etc., Similarly, multi-component reactions (MCR) also address these challenges with simpler procedures utilizing three or more reactants in a single reaction flask to generate a product with most of the atoms in the starting materials [26]. In the way of our commitment towards the development of bioactive molecules [27] and in view of above-mentioned prominence of alkylating groups and synthetic feasibility, herein we proposed aryl α-haloacrylamide-linked dihydropyrimidinone derivatives with the introduction of the alkylating group at C6 position to increase the interactions with cysteine residues (Fig. 2). Furthermore, the newly synthesized derivatives were also evaluated for their *in vitro* antiproliferative activities on selected cancer cell lines and tubulin polymerization inhibition.

2. Results and discussion

2.1. Chemistry

The synthesis of desired derivatives **6a–s** and **10a–g** were depicted in Scheme 1 and 2. 6-Chloro methyl dihydropyrimidinones **4a–g** were synthesized by Biginelli reaction between substituted aromatic aldehydes **2a–g**, 4-chloro ethyl acetoacetate and urea in presence of conc. HCl in ethanol as solvent. Similarly, this reaction was also performed with heterocyclic aldehydes **2h** and **2i**, 4-chloro ethyl acetoacetate and urea in the presence of zinc chloride in THF [28]. These derivatives were subsequently undergoes nucleophillic substitution with different monocyclic and bicyclic phenolic alcohols using K_2CO_3 in acetonitrile to provide ether bridged dihydropyrimidinones **6a–s**. The nitro group was reduced to its corresponding amine in the presence of Fe-powder and anhydrous $CaCl_2$ in 10:1 (v/v) of ethanol: H_2O, followed by coupling with bromoacrylic acid using EDC in DMF to afford the desired bromoacrylamide-linked dihydropyrimidinone derivatives **10a–g** (Scheme 2).

All the synthesized derivatives were carefully analyzed by using HRMS, ^{1}H, ^{13}C NMR and FT-IR. The most potent compound **10f** was characterized by ^{1}H NMR and showed a sharp singlet at δ 10.16 ppm which details the proton after amidation reaction. The two signals at δ 6.73 and 6.28 ppm correspond to the olefinic protons of bromoacrylic acid. Protons of $-CH_2-$ which is adjacent to phenoxy group resonated as a multiplet at δ 5.21 and 5.17 ppm. The triplet and quartet of five protons each at δ 4.00 and 1.06 ppm belong to the $-CH_3-$ and $-CH_2-$ of ester protons respectively. The two singlets of each signal at δ 9.18 and 7.80 ppm account for the N−H protons of cyclic urea of pyrimidinone ring. Characteristic methyl protons appeared as a singlet at δ 2.27 ppm and rest of the protons lie in the aromatic region at δ 7.57–6.96 ppm. Similarly, ^{13}C NMR interpretation of compound **10f** details the presence of carbonyl carbon at δ 165.1 ppm. The methyl and methylene carbons of the ester group were resonated at δ 14.3 and 54.2 ppm respectively. The signal such as $-CH_2-$ adjacent to the phenoxy ring was appeared at δ 60.2 ppm. Tertiary carbon of pyrimidinone ring showed a characteristic peak at δ 64.5 ppm and all the remaining carbons resonates from δ 161.1–102.1 ppm. The spectroscopic data (^{1}H and ^{13}C NMR) of all other newly synthesized derivatives are in agreement with the respective structures as depicted in the experimental

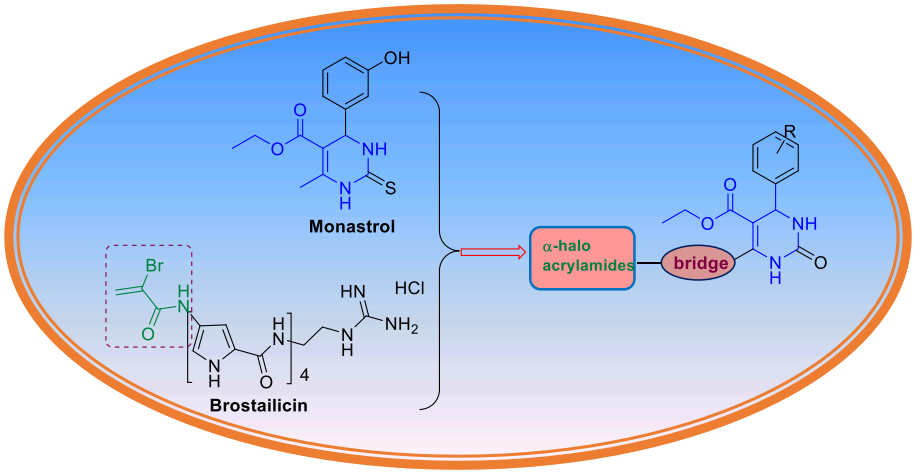

Fig. 2. Design of aryl α-haloacrylamide-linked dihydropyrimidinone derivatives.

section. The HRMS (ESI) of all the compounds showed an $[M + H]^+$ or $[M+2]^+$ peaks corresponding to their respective molecular formula.

2.2. Biological evaluation

2.2.1. Evaluation of in vitro cytotoxic effects

The newly synthesized dihydropyrimidinone derivatives **6a–s** and **10a–g** were screened for their cytotoxicity against various human cancer cell lines MCF-7 (human breast cancer), MDA-MB-231 (human breast cancer), HCT-116 (human colon cancer), HCT-15 (human colorectal adenocarcinoma), HT-29 (human colon adenocarcinoma) and DU145 (human prostate cancer) along with normal lung fibroblasts (HFL-1) purchased from American Type Culture Collection (ATCC) USA, by utilizing 3-(4,5-dimethylthiazol-2-yl)-2,5-diphenyltetrazolium bromide (MTT) assay. The IC_{50} (μM) values from the *in vitro* cytotoxic evaluation of the synthesized derivatives **6a–s** and **10a–g** as well as standard drugs were implied in Table 1. Remarkably, the tested derivatives showed good to moderate cytotoxicity on the selected cancer cell lines. Note worthily, preliminary results indicated that among the acrylamide series, all the derivatives **10a–g**, showed significant

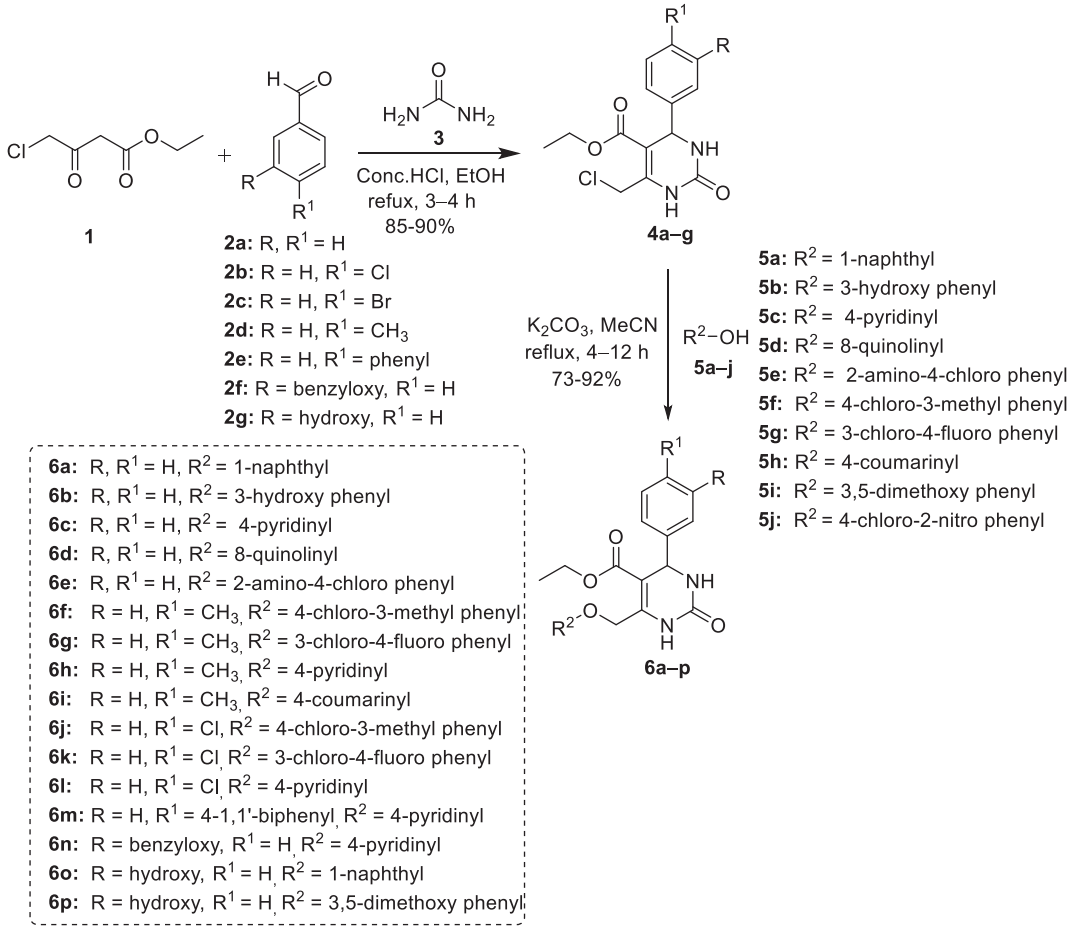

Scheme 1. Synthesis of ethyl 2-oxo-6-(phenoxymethyl)-4-phenyl-1,2,3,4-tetrahydropyrimidine-5-carboxylate derivatives **6a–p**.

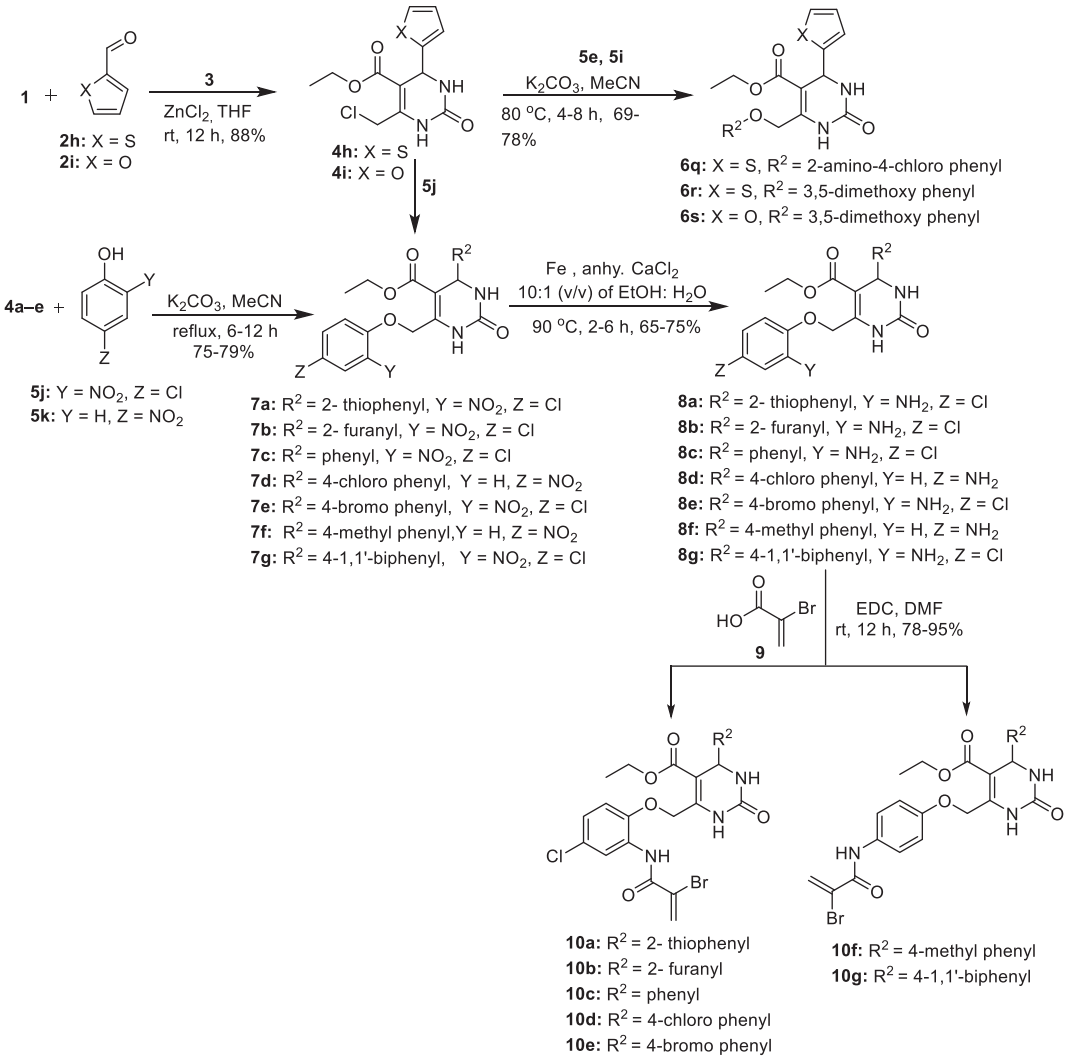

Scheme 2. Synthesis of five-membered and α-haloacrylamide based 1, 2, 3, 4-tetrahydropyrimidine-5-carboxylate derivatives **6q–s** & **10a–g**.

antiproliferative activities against the tested cancer cell lines and the ether bridged series **6a–s** of dihydropyrimidinone showed moderate antiproliferative activities with the IC_{50} values 7.21 ± 1.46 μM to 40.0 μM and above. Among the ether bridged series, derivatives **6i** possessing heterocyclic coumarin ring was active with an IC_{50} value of 7.21 ± 1.46 μM and 7.52 ± 0.28 μM against HCT15 and DU145 respectively. Derivative **6j** with substitution of 4-chloro 3-methyl phenyl was found to be active on prostate cancer cell line (DU145). Furthermore, derivative **6p** derived from monastrol was found to be active against HCT-116 and MDA-MB-231 cell lines with an IC_{50} value of 13.85 ± 0.25 μM and 15.21 ± 1.49 μM, respectively.

Interestingly, the synthesized compounds **10a–g** of acrylamide derivatives showed potent *in vitro* antiproliferative activities against all the tested cancer cell lines with the IC_{50} value ranging from 0.54 ± 0.12 to 8.35 ± 0.82 μM. Although compound **10e** has shown an exceptional IC_{50} of 24.60 ± 1.52 μM on HCT-15 colon cancer cell line. From the precise investigation of the IC_{50} values, it was inferred that the derivative **10f** was more potent to bring about cytotoxicity on all the tested cancer cell lines. It was found to be most significant against MCF-7 breast cancer cell line with an IC_{50} value 0.54 ± 0.12 μM in as much as in MDA-MB-231 breast cancer cell line 50% inhibition was observed at 1.18 ± 0.32 μM. This derivative also found to be active in prostate (DU145) and colon cancer (HCT-116, HCT-15, HT-29) with IC_{50} value of 2.50 ± 0.19 μM, 2.66 ± 0.11 μM, 3.78 ± 0.40 μM and 6.36 ± 0.20 μM respectively. It could be observed from the *in vitro* cytotoxicity studies that compounds bearing five-membered heterocyclic rings thiophenyl (**10a**), furanyl (**10b**) showed potent to moderate cytotoxicity ranging from 1.72 ± 0.12 μM to 8.17 ± 1.02 μM against all the tested cancer cell lines. Substitution of a bulky group such as phenyl (**10g**) also displayed significant cytotoxicity against breast (MCF-7, MDA-MB-231) and prostate cancer cell lines (DU145) with an IC_{50} value of 1.57 ± 0.28 μM, 1.06 ± 0.14 μM and 1.50 ± 0.25 μM respectively. It is evident from IC_{50} values that the position of acrylamide on dihyropyrimidinone ring has not greatly influenced the cytotoxicity but ether bridge containing acrylamide at the *para* position has displayed remarkable cytotoxicity on all the tested cancer cell lines. Notably, in MDA-MB-231 and MCF-7 breast cancer cell lines, compounds **10a–g** exhibited potent antiproliferative activities with the IC_{50} value ranging from 0.54 ± 0.12 to 3.70 ± 0.24 μM, which presumes that these results may help in identification of new anti-breast cancer agents with enhanced activity. Based on the *in vitro* cytotoxicity, the Structure Activity Relationship (SAR) of the entitled compounds was constructed and represented in Fig. 3 and the most potent compound **10f** was selected for further studies towards the mechanism of cancer cell growth inhibition and tubulin polymerization inhibition.

2.3. Effect of 10f on tubulin polymerization inhibition

To investigate the inhibitory activity of **10f** by its interactions with microtubule system [29], the tubulin polymerization inhibitory potential was evaluated for **10f** at different concentrations (10, 5, 2.5, 1.25,

Table 1
IC_{50} (μM) values[a] against human cancer cell lines by derivatives **6a–s** and **10a–g** by MTT assay.

Compound	MCF7[b]	MDA-MB-231[c]	HCT -116[d]	HCT-15[e]	HT 29[f]	DU145[g]	HFL-1[h]
6a	35.40 ± 0.42	29.14 ± 1.26	23.62 ± 0.89	30.12 ± 1.36	> 50	39.34 ± 0.74	34.06 ± 6.41
6b	25.26 ± 0.16	36.83 ± 0.16	33.89 ± 0.25	40.21 ± 0.24	39.12 ± 1.43	47.74 ± 0.43	33.69 ± 6.95
6c	26.72 ± 0.22	40.15 ± 1.22	35.47 ± 0.44	29.83 ± 0.58	30.71 ± 0.84	43.81 ± 1.31	41.28 ± 5.86
6d	> 50	28.95 ± 1.05	29.12 ± 1.65	28.46 ± 0.63	> 50	40.01 ± 0.61	38.23 ± 9.87
6e	28.60 ± 1.45	40.87 ± 0.83	29.45 ± 0.32	36.85 ± 0.17	28.95 ± 1.37	38.48 ± 0.72	37.23 ± 8.12
6f	34.56 ± 0.78	29.63 ± 0.83	28.89 ± 1.54	31.60 ± 0.87	30.71 ± 0.85	33.58 ± 0.62	31.32 ± 9.76
6g	29.43 ± 0.36	> 50	39.46 ± 0.68	26.75 ± 0.24	26.72 ± 0.28	28.89 ± 1.93	48.69 ± 9.57
6h	27.48 ± 0.34	38.73 ± 0.83	34.53 ± 0.76	34.42 ± 1.85	25.19 ± 0.90	29.48 ± 0.39	53.03 ± 3.15
6i	29.62 ± 1.83	43.19 ± 1.17	40.54 ± 1.15	7.21 ± 1.46	29.84 ± 0.56	7.52 ± 0.28	52.85 ± 8.16
6j	38.14 ± 1.24	35.92 ± 1.20	28.11 ± 0.22	28.61 ± 1.43	28.62 ± 1.44	11.85 ± 1.29	47.86 ± 14.23
6k	39.26 ± 1.21	> 50	40.22 ± 0.23	39.13 ± 1.41	> 50	23.01 ± 1.61	34.94 ± 6.95
6l	> 50	38.82 ± 0.27	36.87 ± 0.15	25.25 ± 0.12	25.23 ± 0.16	30.17 ± 0.58	48.01 ± 4.20
6m	33.83 ± 0.26	35.44 ± 0.45	25.23 ± 0.17	33.89 ± 0.27	28.47 ± 0.69	27.44 ± 0.73	41.39 ± 9.41
6n	> 50	48.82 ± 1.66	36.80 ± 0.19	40.22 ± 0.29	39.18 ± 1.42	30.75 ± 0.68	29.42 ± 6.28
6o	28.41 ± 0.68	25.49 ± 0.43	> 50	26.77 ± 0.25	35.47 ± 0.43	29.80 ± 0.51	47.17 ± 3.63
6p	40.84 ± 1.61	15.21 ± 1.49	13.85 ± 0.25	35.46 ± 0.66	38.11 ± 1.20	29.17 ± 1.69	29.25 ± 0.60
6q	25.62 ± 0.32	38.84 ± 1.21	40.21 ± 0.22	29.64 ± 1.83	29.46 ± 0.34	30.34 ± 0.92	39.54 ± 2.46
6r	29.12 ± 1.66	43.47 ± 0.16	36.33 ± 0.63	29.88 ± 1.64	> 50	> 50	47.41 ± 6.29
6s	> 50	25.12 ± 0.93	28.94 ± 1.04	> 50	38.8 ± 0.2	29.12 ± 1.27	28.98 ± 8.62
10a	2.18 ± 0.25	1.72 ± 0.12	3.56 ± 0.17	4.70 ± 0.26	8.17 ± 1.02	2.90 ± 0.14	47.63 ± 8.27
10b	3.15 ± 0.72	2.08 ± 0.56	4.43 ± 0.16	5.90 ± 0.13	7.25 ± 0.64	3.80 ± 0.23	35.36 ± 6.84
10c	2.64 ± 0.26	1.83 ± 0.28	5.70 ± 0.18	5.80 ± 0.55	6.60 ± 0.42	1.71 ± 0.25	43.23 ± 6.75
10d	2.65 ± 0.34	1.13 ± 0.12	6.40 ± 0.20	6.17 ± 0.61	8.35 ± 0.82	2.60 ± 0.47	40.63 ± 2.26
10e	3.70 ± 0.24	1.25 ± 0.16	5.70 ± 0.31	24.60 ± 1.52	3.50 ± 0.12	3.30 ± 0.14	29.47 ± 4.50
10f	0.54 ± 0.12	1.18 ± 0.32	2.66 ± 0.11	3.78 ± 0.40	6.36 ± 0.26	2.50 ± 0.19	50.04 ± 11.21
10g	1.57 ± 0.28	1.06 ± 0.14	5.30 ± 0.19	4.30 ± 0.13	7.10 ± 0.25	1.50 ± 0.25	19.28 ± 0.65
5-FU[i]	3.2 ± 0.53	0.6 ± 0.32	1.16 ± 0.062	ND	3.9 ± 1.1	ND	ND
Podoph yllotoxin[i]	ND	0.014 ± 1.21	0.06 ± 0.005	0.08 ± 0.24	0.02 ± 0.98	0.07 ± 0.003	ND
Monastrol[i]	12.9 ± 0.02	ND	ND	ND	> 100	ND	ND

[a] 50% Inhibitory concentration after 72 h of drug treatment, [b,c] Human breast cancer, [d,e,f] Human colon cancer, [g] Human prostate cancer, [h] Human normal lung fibroblasts, [i] Reference compound. All the values are expressed as Mean ± SEM in which each treatment was performed in triplicate wells.

0.625 μM) with podophyllotoxin 5 μM and paclitaxel 3 μM) serving as a positive control. The cell cycle arrest in G2/M phase in most of the cancer cells is frequently associates with the tubulin polymerization inhibition. The compound **10f** also displayed G2/M cell cycle arrest, hence in order to understand the concealed mechanism of the active compound, we performed cell-free *in vitro* tubulin polymerization assay by monitoring the increase in fluorescence emission at 440 nm (excitation wavelength is 360 nm) for 1 h at 37 °C (Fig. 4a). The experiment was performed in duplicates and from the Fig. 4b, it was inferred that 22.4%, 30.5%, 75.3% of tubulin polymerization were observed in the treatment group of **10f** at the concentrations of 2.5, 5.0, and 10.0 μM, respectively, compared to the vehicle group (DMSO). To our delight, the compound **10f** displayed potent tubulin polymerization inhibition with an IC_{50} value of 6.91 ± 0.43 μM and correlated well with the anti-proliferative potency, affirming that the growth of cancer cells was inhibited by **10f** in a dose-dependent manner through the tubulin polymerization inhibition.

3. Molecular docking

To elucidate the binding mode and type of interactions with tubulin (PDB ID: 1SA0), we have performed molecular docking studies with the most active compound **10f** using the GLIDE docking module of Schrödinger suite 2017-1 [30]. From the docking study, it was observed that the top-ranked conformation of compound **10f** was well accommodated inside the colchicine binding site of the tubulin. As shown in Fig. 5a, docking studies suggest that the compound **10f** binds well in the colchicine-binding domain at the α/β-tubulin interface. More detailed analysis of the inhibitor-tubulin complex (Fig. 5b) exposed various hydrogen-bonding interactions that appear to play a key role in the

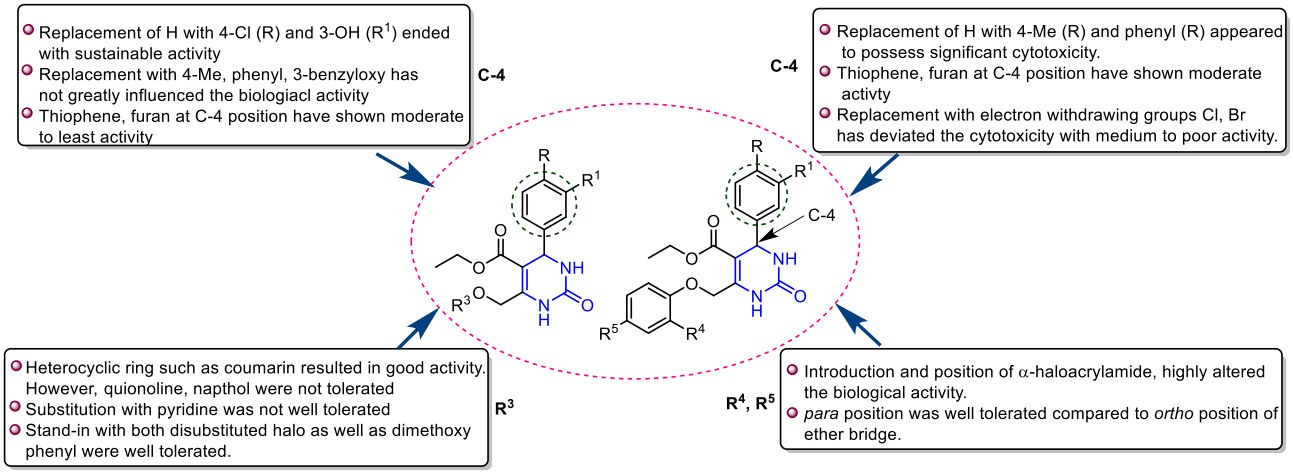

Fig. 3. Structure Activity Relationship (SAR) of aryl α-haloacrylamide and ether-linked dihydropyrimidinone derivatives.

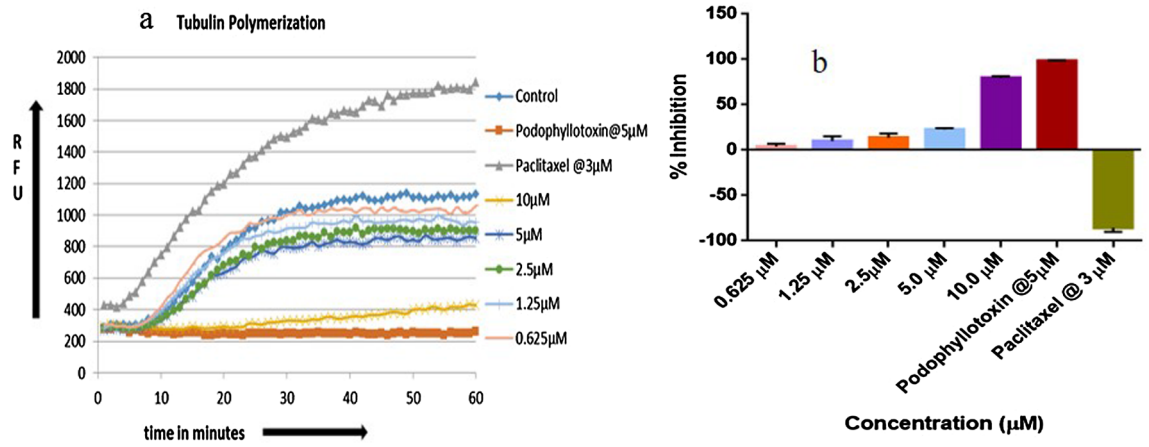

Fig. 4. (a) Effect of compound **10f** on the tubulin polymerization: tubulin polymerization was monitored by the increase in fluorescence at 360 nm (excitation) and 440 nm (emission) for 1 h at 37 °C. (**b**) % Dose-response inhibition of tubulin polymerization by compound **10f** at final concentrations of 10, 5, 2.5, 1.25, 0.625 μM. Podophyllotoxin and paclitaxel, were used as reference standards. Data expressed as mean ± SEM (n = 3).

binding mode. Compound **10f** showed three hydrogen bonding interactions with the catalytically active residues Ser178, Val238 and Val318. The nitrogen atom at N-1 position of dihydropyrimidinone ring acts as hydrogen bond acceptor and involved in the hydrogen bond interaction with back bone NH_2 of Val318 (d ¼ 3.7 Å), and the nitrogen atom at N-3 position of dihydropyrimidinone ring acts as hydrogen bond acceptor and involved in the hydrogen bond interaction with main chain NH_2 of Ser178 (d ¼ 3.5 Å). Similarly, the oxygen atom of ethyl ester showed a hydrogen-bonding interaction with the side chain NH_2 of Val318 (d ¼ 3.6 Å). Additionally, several hydrophobic interactions were observed between the compound **10f** and the active site residues, e.g., Val74, Tyr202, Val238, Cys241, Leu242, Leu248, Ala250, Leu252, Leu255, Met259, Val315, Pro348 and Val351 which stabilizes the binding of the compound **10f** in the colchicine-binding domain of α/β-tubulin interface. To deepen and understand our findings, we tried the superimposition of colchicine with the ligands and the resultant superimposition poses suggest that ether bridged phenyl ring of ligands under investigation occupied identical position with respect to tri-methoxy phenyl ring of colchicine and the carbonyl group of ester in **10f** superimposes with the amide carbonyl of the colchicine as noticed in Fig. 5c.

4. Analysis of cell cycle effect

Most of the chemotherapeutic agents exhibit their growth inhibitory potential by the obstruction of cell cycle sequence at a specific check point [31]. From the *in vitro* cytotoxicity results, it was clear that the compound **10f** displayed noticeable cytotoxicity against MCF-7 breast cancer cells. Cell cycle analysis study was performed, wherein HEK-293 (Human embryonic kidney cells) considered as control and MCF-7 cells were treated with the compound **10f** for 48 h at 0.5 μM. The data obtained clearly indicated that these compounds show cell cycle arrest at the G2/M phase in comparison with the untreated control cells. The **10f** compound showed 22.39% and 31.41% of cell accumulation in G2/M phase at 0.5 μM concentration in MCF-7 cells, whereas they exhibited 17.27% and 18.97% of cell accumulation at 0.5 μM concentration with HEK-293 cells. The cell cycle assay data indicate the accumulation of

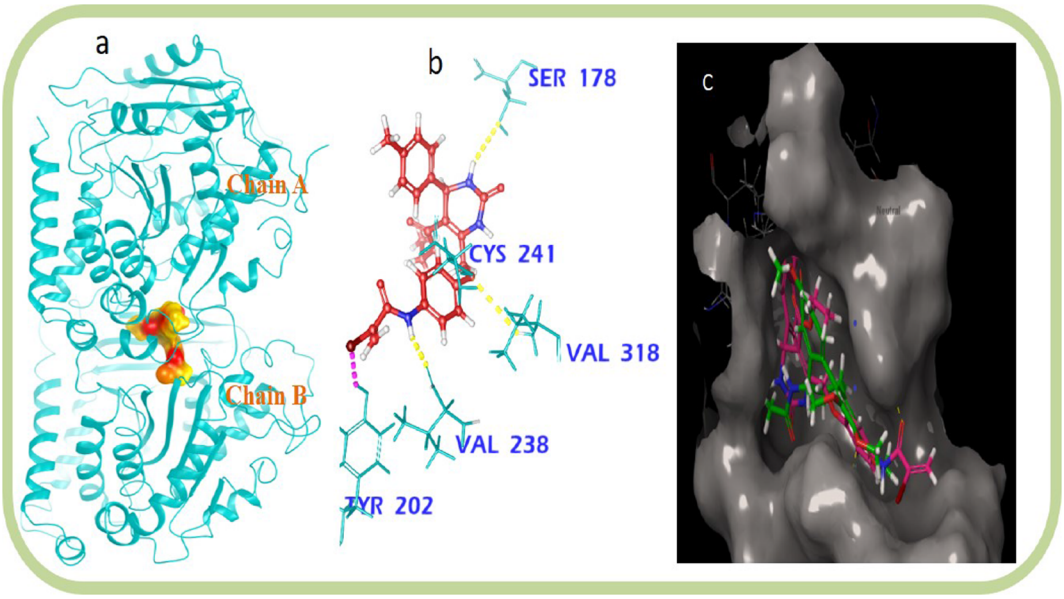

Fig. 5. (a) Docking model of most potent compound **10f** and (**b**) its ligand interactions in the colchicine binding site of α/β-tubulin (PDB ID: 1SA0). The yellow dashed lines represent hydrogen bonds. (c) Poses represent the superimposition of potential ligands (**10f**) and colchicine at the colchicine binding domain: The potential ligands were shown as ball and stick model, while the interacting aminoacids were denoted as thin tubes and the colchicine was shown as green ball and stick model in the black background.

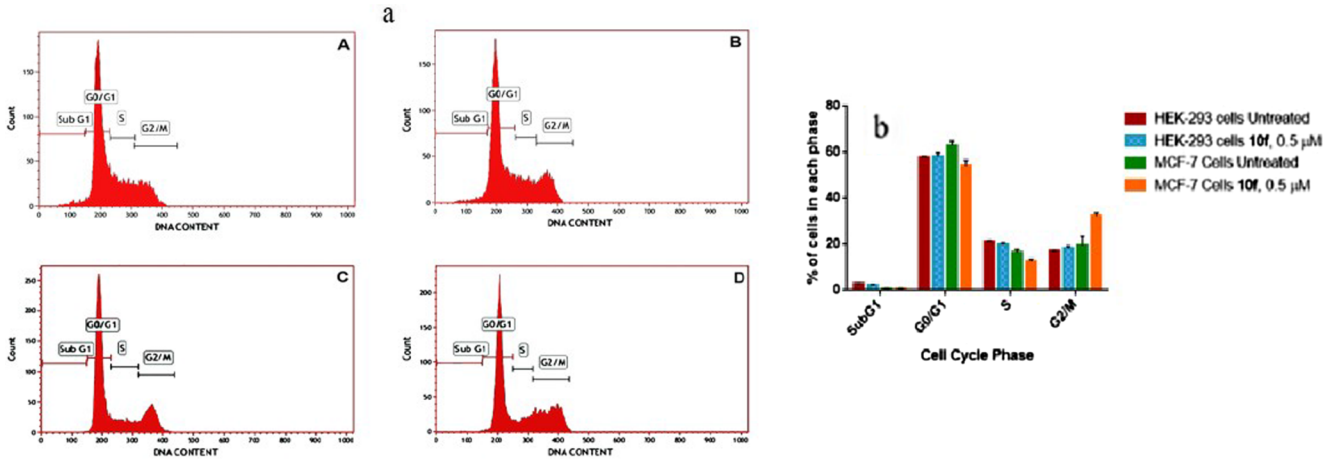

Fig. 6. (a) Cell cycle analysis showing the effect of **10f** on HEK-293 (control cells) and MCF-7 cells 48 h. **A**. Untreated HEK-293 cells **B**. HEK-293 cells after treatment with 0.5 µM **10f C**. Untreated MCF-7 cells **D**. MCF-7 cells after treatment with 0.5 µM **10f**. The cell cycle assay was performed by Propidium Iodide (PI) staining method. (b) Effect of % Dose-response inhibition by compound **10f** at a concentration of 0.5 µM in different phases of cell cycle. Data expressed as mean ± SEM (n = 3).

MCF-7 cells at G2/M phase on the treatment of cells with 0.5 µM of compound **10f** (Fig. 6a and b). Further, there is no change in the percentage of HEK-293 cells at G2/M phase even after the treatment with 0.5 µM of compound **10f**.

5. Apoptosis detection studies

5.1. Identification of apoptotic cells

DAPI (4',6-diamidino-2-phenylindole) is a dominant chromosome counter stain, binds immutably to the AT clusters in the minor groove of DNA, by reason of which it reveals the nuclear contraction through chromatin condensation. DAPI penetrates less efficiently into the flawless membrane in comparison to the disintegrated membrane and thereby figure out the apoptotic cells from the live ones. Hence, apoptotic cells appear brighter rather than live cells. Therefore, it is of high value to study the nuclear damage induced by compound **10f** in MCF-7 by staining with DAPI [32]. As shown in Fig. 7 in the control (a), the living cells show normal morphology and the cell nuclei preserve intact. However, MCF-7 cells were treated with 0.5 µM (b), 1 µM (c), 2.0 µM (d) and 4.0 µM (e) of **10f** for 72 h, the cells exhibit the representative apoptotic features including nuclear shrinkage, pyknotic or fragmented bright nuclei, and chromatin condensation.

5.2. Detection of morphology during apoptosis induction

Dual AO/EB staining is a simple method to identify apoptosis-associated changes of cell membranes during the process of apoptosis thereby helpful in tumor drug sensitivity test. AO can efficiently infiltrate the immaculate membrane and smears the nuclei green, while EB can only infuse disrupted cell membrane and stain the nucleus red [33]. This study is generally used to differentiate the apoptotic, necrotic and live cells. From Fig. 8, it can be inferred that the cell population in control exhibited the regular morphology and appeared green in color. However, **10f** treated MCF-7 cells clearly disclosed the distorted morphological characteristics such as cell contraction, membrane blebbing, chromatin condensation and apoptotic body formation implying that the compound had induced apoptosis in a dose-dependent manner.

5.3. Quantification of apoptosis induction

Annexin V-FITC/Propidium iodide dual staining assay expedites the quantification of apoptotic cell death using flow cytometry. This assay simplifies the identification of necrotic cells (Q1-UL; AV-/PI+), late apoptotic cells (Q1- UR; AV+/PI+), early apoptotic cells (Q3-LR; AV+/PI-) and live cells (Q2-LL; AV-/PI-) [34]. MCF-7 breast cancer cells were treated with compound **10f** at different concentrations of 0.25, 0.5, and 1 µM for 72 h. It can be observed from Fig. 9a that the percentage of late and early apoptotic cells significantly enhanced with an increase in the concentration of compound **10f**, which represents the dose-dependent apoptosis induction Fig. 9b on MCF-7 breast cancer cells.

5.4. Effect on mitochondrial membrane potential (DΨm)

Disruption of active mitochondria is the unique peculiarity of the initial stage of programmed cell death. Alterations in the oxidation-reduction potential of the mitochondrial membrane lead to the enhanced generation of reactive oxygen species (ROS) and thereby loss of mitochondrial membrane potential (DΨm) [35]. Therefore, it is a decisive task to study the effect of compound **10f** on mitochondrial membrane potential (DΨm). The membrane-permeate JC-1 dye was used for determining DΨm, in which J-aggregates in healthy mitochondria, therefore, stains red in color whereas depolarized mitochondria consist of J-monomers so they will stain in green. MCF-7 cells were treated with compound **10f** at different concentrations for 72 h and then subjected to JC-1 staining. Flow cytometric analysis revealed that the compound **10f** caused a noteworthy enhancement in the depolarized cell population i.e., J-monomers from control 1.82 to 91.38% at 2.0 µM in a dose-dependent manner as shown in Fig. 10.

5.5. Effect of 10f on intracellular ROS generation

Enhanced free radical generation is believed to contribute to the damage of mitochondrial potential due to oxidative stress and thereby leads to apoptosis [36]. Hence, to examine the degree of ROS generation by compound **10f**, the intracellular ROS generation was driven using the DCFDA staining. MCF-7 cells were treated with increased doses of compound **10f**, where increased green fluorescence proportionality is observed with increase in the concentration, in which DCFDA is oxidized to 2′,7′-dichlorofluorescein (DCF) in the presence of ROS generation. From Fig. 11, it surely indicates the potential of **10f** in inducing ROS generation as compared to the control and thereby it could be one of the mechanisms considered in prompting apoptosis in MCF-7 breast cancer cells.

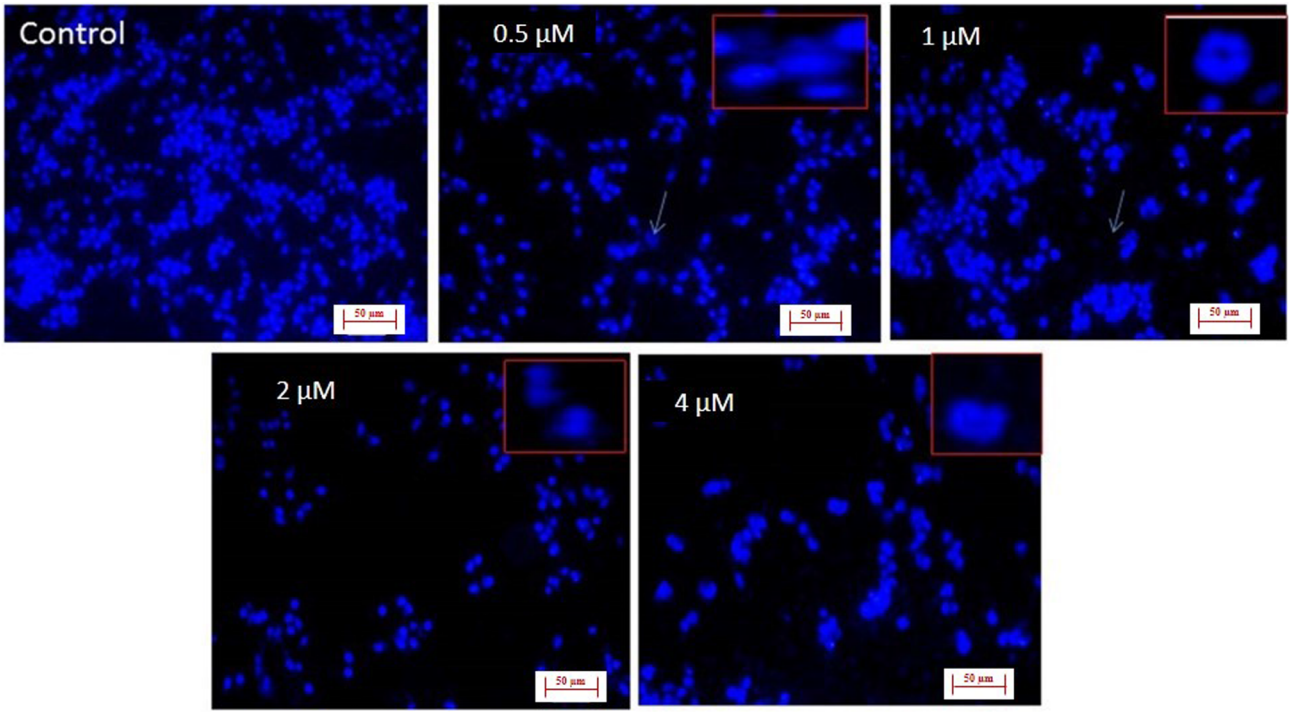

Fig. 7. Effect of **10f** on nuclear morphology of cancer cells after DAPI staining. Breast cancer (MCF-7) cells treated with and without compound **10f** at various concentrations 0.5, 1, 2 and 4 µM for 72 h and compared with control. The images were captured with fluorescence microscope at 200X. Red scale Bar in the image indicates 50 µm.

6. Conclusion

In conclusion, a new series of dihydropyrimidinone derivatives were designed and synthesized by employing multi-component Biginelli reaction with the introduction of α-haloacrylamide at the 6th position through ether linked mono and bicyclic frameworks. Later, *in vitro* cytotoxic potential for these derivatives were screened against a selected panel of human cancer cell lines. From the preliminary screening, it was inferred that compound **10f** displayed a substantial biological response against all the tested cancer cell lines specifically on MCF-7 breast cancer cell line with IC_{50} of 0.54 ± 0.1 µM. Induction of apoptosis was evident by AO/EB staining, DAPI nuclear staining, and Annexin V/Propidium Iodide assay. Compound **10f** caused the collapse of mitochondrial membrane potential (ΔΨM), elevated generation of ROS

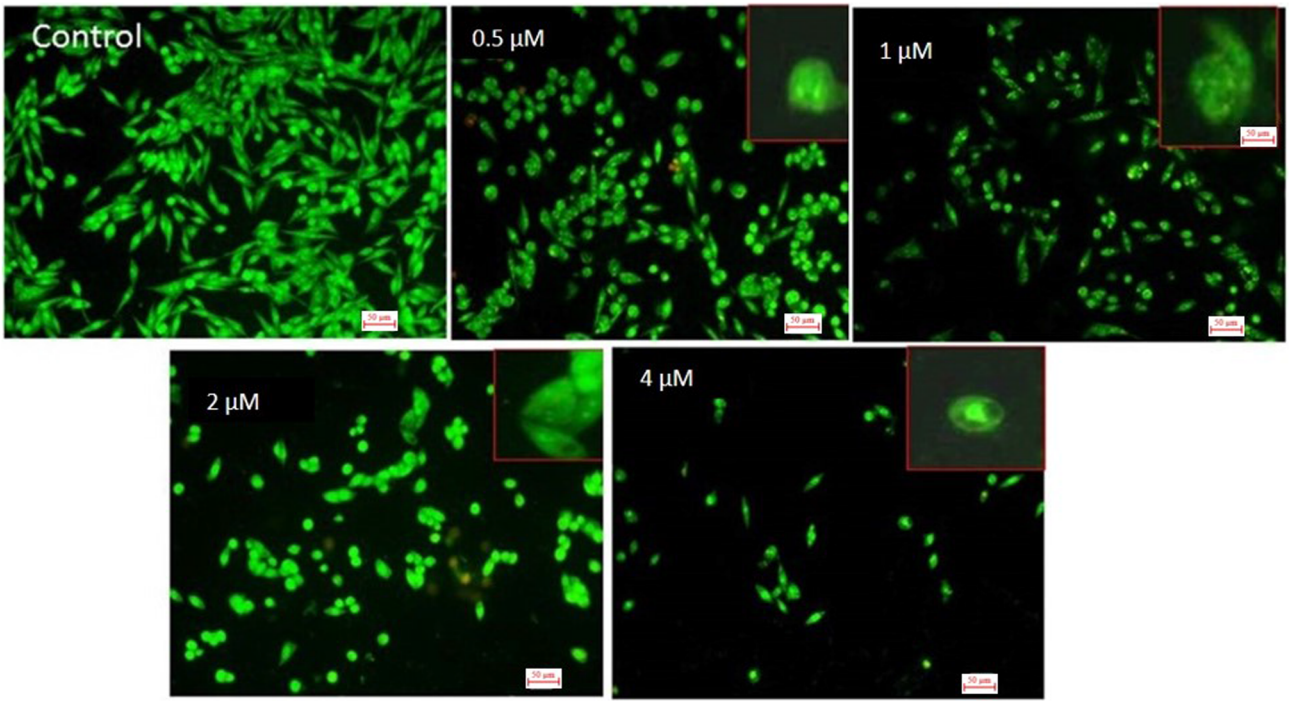

Fig. 8. AO/EB staining in breast cancer cells (MCF-7), cells treated with and without compound **10f** at various concentrations 0.5, 1, 2 and 4 µM for 72 h and compared with control. The images were captured with fluorescence microscope at 200X. Red scale Bar indicates 50 µm.

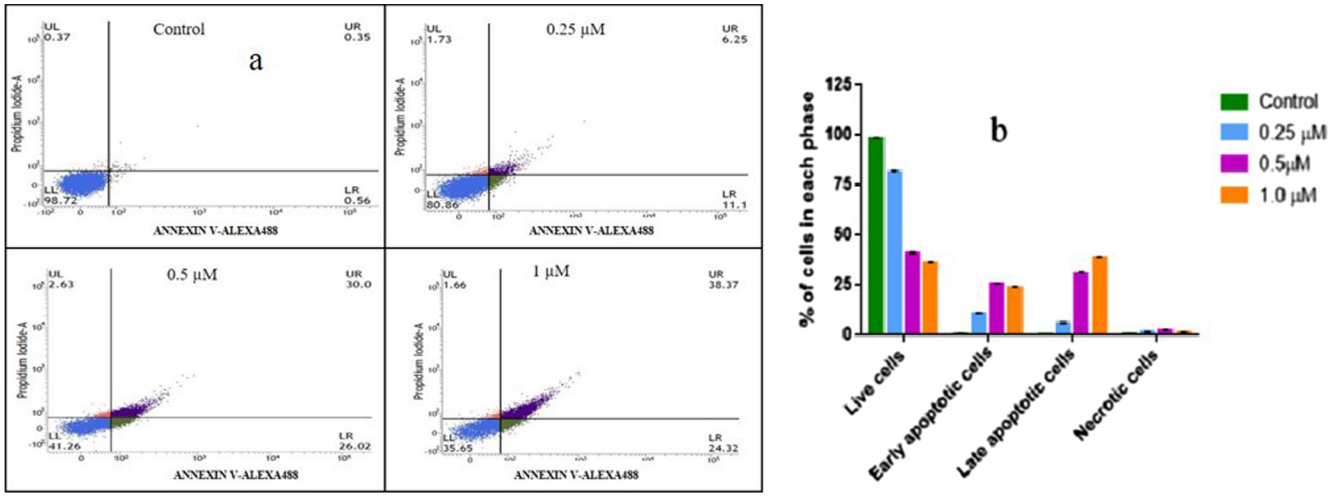

Fig. 9. (a) Effect of compound **10f** on cell apoptosis induction of MCF-7 cells was measured by Annexin V-Alexa Flour 488/propidium iodide staining assay. MCF-7 cells were treated with compound **10f** ranging from 0.25 to 1.0 µM concentration and control (untreated cells) for 72 h. Then 10,000 cells from each sample were analyzed by flow cytometry. The percentage of cells positive for Annexin V-Alexa Flour 488 and/or Propidium iodide is represented inside the quadrants. Cells in the upper left quadrant (Q1-UL; AV-/PI+): necrotic cells; lower left quadrant (Q2-LL; AV−/PI−): live cells; lower right quadrant (Q3-LR; AV+/PI−): early apoptotic cells and upper right quadrant (Q4- UR; AV+/PI+): late apoptotic cells. (**b**) % Dose-response inhibition by compound **10f** at final concentrations of 0.25, 0.5, 1 µM. Data expressed as mean ± SEM (n = 3).

and cell cycle arrest at G2/M phase in MCF-7 cancer cell line in a dose dependent manner. Molecular modelling studies supported the possible binding mode of action by **10f** to the α/β-tubulin. In addition, compound **10f** inhibited tubulin polymerization by 50% at a concentration of 6.91 ± 0.43 µM in an *in vitro* assay with microtubule-destabilizing properties. Overall, the current studies demonstrate that the new α-haloacrylamide-linked dihydropyrimidinone derivatives can be developed as potent tubulin inhibitors and their further structural modifications may generate promising new anti-breast cancer leads in cancer therapy.

7. Experimental section

7.1. Chemistry

General Methods. All the reagents and solvents were obtained from commercial suppliers and were used without further purification. Analytical thin layer chromatography (TLC) was performed on MERCK pre-coated silica gel 60-F254 (0.5 mm) aluminum plates. Visualization of the spots on TLC plates was achieved by UV light. ^{1}H and ^{13}C NMR spectra were recorded on Bruker 500 MHz by making a solution of

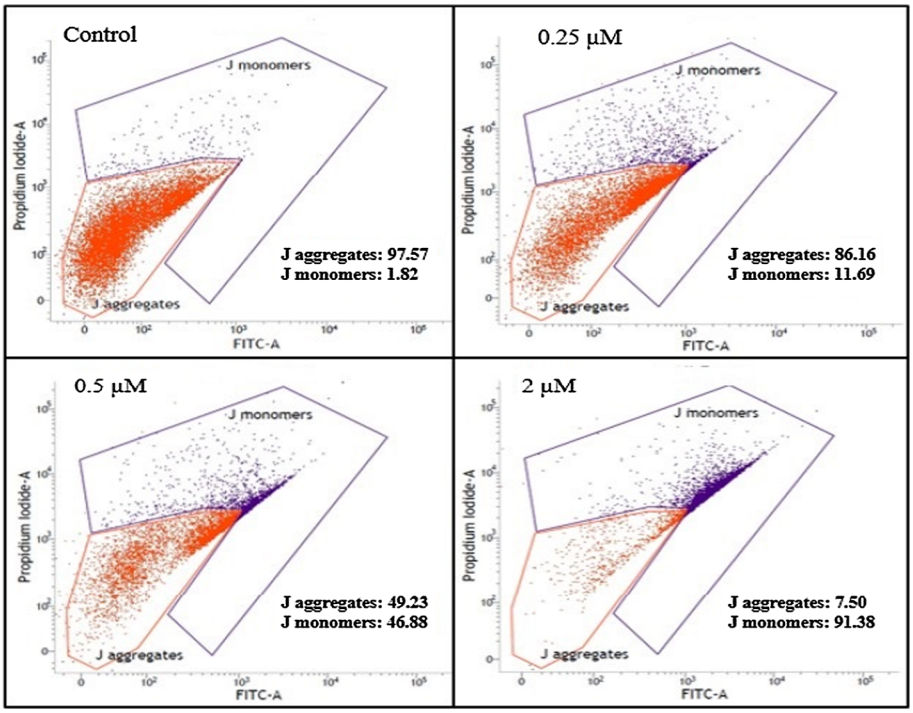

Fig. 10. Effect on mitochondrial membrane potential. MCF-7 cells were treated with various concentrations (0.25, 0.5, 2 µM) of compound **10f** for 72 h and JC-1 staining was performed. The control represents the cells without compound **10f** treatment.

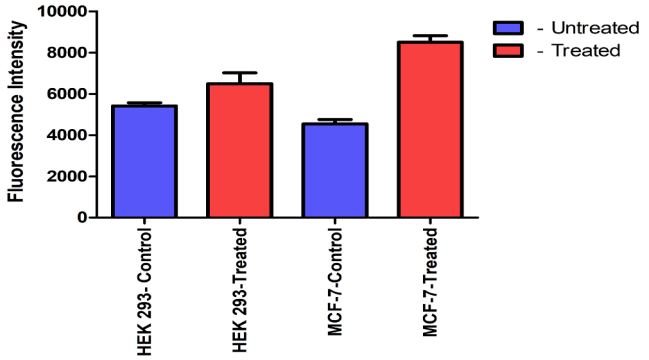

Fig. 11. ROS generated before and after the treatment of **10f** to HEK-293 and MCF-7 cells. Data expressed as mean ± SEM (n = 3).

samples in the DMSO-d_6 as solvent using tetramethyl silane (TMS) as the internal standard. Chemical shifts for ^{1}H and ^{13}C are reported in parts per million (ppm) downfield from tetra methyl silane. Spin multiplicities are described as s (singlet), brs (broad singlet), d (doublet), t (triplet), q (quartet), and m (multiplet). Coupling constant (*J*) values are reported in *hertz* (Hz). HRMS were determined with Agilent QTOF mass spectrometer 6540 series instrument. Wherever required, column chromatography was performed using silica gel (60–120). The reactions wherever anhydrous conditions required are carried under nitrogen positive pressure using freshly distilled solvents. All evaporation of solvents was carried out under reduced pressure using rotary evaporator below 45 °C. Melting points were determined with an electro thermal digital melting point apparatus IA9100 and are uncorrected. The names of all the compounds given in the experimental section were taken from ChemBioDraw Ultra, Version 12.0.

*7.1.1. Ethyl 2-oxo-6-(aryloxymethyl)-4-aryl/heteroaryl-1,2,3,4-tetrahydropyrimidine-5-carboxylate (**6a–s**)*

To a mixture of chlorinated derivatives of dihydropyrimidinone derivatives **4a–i** (1 equiv.), potassium carbonate (2.5 equiv.) in acetonitrile, under 80 °C was added different aryl/ heteroaryl alcohols (**5a–k**, 0.75 equiv.) and stirred under reflux till complete consumption of the starting materials as determined by TLC. The solvent was then removed using rotary evaporator and extracted using ethyl acetate (25 mL × 3) and water. The organic layer was concentrated under *in vacuo* and the residue obtained was chromatographed on silica gel (elution with hexane/EtOAc = 7:3–5:5) to provide the 2-oxo-6-(aryloxymethyl)-4-aryl/heteroaryl-1,2,3,4-tetrahydropyrimidine-5-carboxylate derivatives ***6a–s*** in moderate to good yields.

*7.1.1.1. Ethyl 6-((2-(2-bromoacrylamido)-phenoxy)methyl)-2-oxo-4-aryl-1,2,3,4-tetrahydro pyrimidine-5-carboxylate (**10a–g**).* To a mixture of 2-bromoacrylic acid (**9**, 1 equiv.), ethyl 6-(phenoxy methyl)-2-oxo-4-aryl-1,2,3,4-tetrahydropyrimidine-5-carboxylate amines (**8a–g**, 1 equiv.), in DMF, EDC (2 equiv.) was added and stirred at 25 °C till complete consumption of the starting materials as determined by TLC. The reaction mixture was then quenched with ice-cold water and extracted using ethyl acetate (25 mL × 3). The organic layer was concentrated under *in vacuo* and the residue obtained was chromatographed on silica gel (elution with hexane/EtOAc = 6:4–4:6) to provide the bromoacrylamido-4-phenoxymethyl-2-oxo-4-phenyl-1,2,3,4-tetrahydropyrimidine-5-carboxylate derivatives in moderate to good yields.

*7.1.1.2. Ethyl 6-((naphthalen-2-yloxy)methyl)-2-oxo-4-phenyl-1,2,3,4-tetrahydropyrimidine-5-carboxylate (**6a**).* White solid; yield 89%; mp:185–189 °C; FT-IR (cm^{-1}): 2922, 2862, 1897, 1710, 1370, 738; ^{1}H NMR (500 MHz, DMSO-d_6): δ 9.32 (s, 1H), 7.87 (d, *J* = 5.1 Hz, 2H), 7.85 (s, 1H), 7.80 (d, *J* = 8.2 Hz, 1H), 7.50–7.46 (m, 1H), 7.40–7.35 (m, 2H), 7.32–7.31 (m, 1H), 7.30 (d, *J* = 6.2 Hz, 3H), 7.28–7.26 (m, 2H), 5.33 (d, *J* = 11.9 Hz, 1H), 5.24 (d, *J* = 3.4 Hz, 1H), 5.16 (d, *J* = 12.0 Hz, 1H), 4.03–3.99 (m, 2H), 1.04 (t, *J* = 7.1 Hz, 3H); ^{13}C NMR (125 MHz, DMSO-d_6): δ 165.2, 156.3, 152.4, 146.1, 144.5, 134.5, 129.7, 129.2, 128.9, 128.0, 128.0, 127.2, 126.9, 126.8, 124.3, 119.2, 107.5, 102.0, 64.3, 60.3, 54.5, 14.3; HRMS (ESI): *m/z* calc. for $C_{24}H_{22}N_2O_4$ 403.1658; found 403.1674 $[M+H]^+$.

*7.1.1.3. Ethyl 6-((3-hydroxyphenoxy)methyl)-2-oxo-4-phenyl-1,2,3,4-tetrahydropyrimidine-5-carboxylate (**6b**).* White solid; yield 82%; mp:183–186 °C; FT-IR (cm^{-1}): 2922, 2876, 1834, 1715, 1693, 1487, 754; ^{1}H NMR (500 MHz, DMSO-d_6): δ 9.23 (s, 1H), 7.85 (s, 1H), 7.43–7.31 (m, 4H), 7.31–7.20 (m, 4H), 6.67–6.61 (m, 2H), 5.23–5.20 (m, 2H), 4.97 (d, *J* = 12.0 Hz, 1H), 4.00–3.97 (m, 2H), 1.04 (t, *J* = 7.1 Hz, 3H); ^{13}C NMR (125 MHz, DMSO-d_6): δ 165.1, 159.6, 152.3, 146.0, 144.5, 130.4, 128.9, 127.9, 126.7, 107.9, 102.3, 101.9, 64.3, 60.2, 54.5, 14.3; HRMS (ESI): *m/z* calculated for $C_{20}H_{20}N_2O_5$ 369.1450 found 369.1483 $[M+H]^+$.

*7.1.1.4. Ethyl 2-oxo-4-phenyl-6-((pyridin-4-yloxy)methyl)-1,2,3,4-tetrahydropyrimidine-5-carboxylate (**6c**).* Yellow solid; yield 88%; mp:178–182 °C; FT-IR (cm^{-1}): 2927, 2868, 1839, 1788, 1367, 758; ^{1}H NMR (500 MHz, DMSO-d_6): δ 7.68 (d, *J* = 6.9 Hz, 2H), 7.41–7.13 (m, 6H), 7.03 (s, 1H), 6.06 (d, *J* = 6.9 Hz, 2H), 5.14 (s, 1H), 5.06 (d, *J* = 13.7 Hz, 1H), 4.92 (d, *J* = 13.7 Hz, 1H), 4.06–3.88 (m, 2H), 1.08 (t, *J* = 6.8 Hz, 3H); ^{13}C NMR (125 MHz, DMSO-d_6): δ 177.7, 165.7, 146.2, 141.4, 128.6, 127.5, 126.7, 117.6, 59.6, 55.1, 54.8, 14.5; HRMS (ESI): *m/z* calculated for $C_{19}H_{19}N_3O_4$ 354.1454 found 354.1450 $[M+H]^+$.

*7.1.1.5. Ethyl 2-oxo-4-phenyl-6-((quinolin-8-yloxy)methyl)-1,2,3,4-tetrahydropyrimidine-5-carboxylate (**6d**).* White solid; yield 79%; mp:183–185 °C; FT-IR (cm^{-1}): 2927, 2856, 1839, 1788, 1367, 748; ^{1}H NMR (500 MHz, DMSO-d_6): δ 9.43 (s, 1H), 9.28 (s, 1H), 7.83 (d, *J* = 8.7 Hz, 2H), 7.75 (d, *J* = 8.6 Hz, 1H), 7.48 (d, *J* = 6.9 Hz, 1H), 7.40–7.34 (m, 2H), 7.29 (d, *J* = 8.9 Hz, 1H), 7.11 (t, *J* = 7.8 Hz, 1H), 6.76–6.70 (m, 2H), 6.66 (d, *J* = 8.1 Hz, 1H), 5.34 (d, *J* = 11.9 Hz, 1H), 5.17 (d, *J* = 3.4 Hz, 1H), 5.09 (d, *J* = 11.9 Hz, 1H), 4.06–4.00 (m, 2H), 1.07 (t, *J* = 7.1 Hz, 3H); ^{13}C NMR (125 MHz, DMSO-d_6): δ 165.2, 156.3, 152.4, 146.1, 144.5, 134.5, 129.7, 129.2, 128.9, 128.0, 128.0, 127.2, 126.9, 126.8, 124.3, 119.2, 107.5, 102.0, 64.3, 60.3, 54.5, 14.3; HRMS (ESI): *m/z* calculated for $C_{23}H_{21}N_3O_4$ 404.1610 found 404.1632 $[M+H]^+$.

*7.1.1.6. Ethyl 6-((2-amino-4-chlorophenoxy)methyl)-2-oxo-4-phenyl-1,2,3,4-tetrahydropyrimidine-5-carboxylate (**6e**).* White solid; yield 82%; mp:179–184 °C; FT-IR (cm^{-1}): 2949, 2832, 1837, 1768, 1347, 774; ^{1}H NMR (500 MHz, DMSO-d_6): δ 9.29 (s, 1H), 7.84 (s, 1H), 7.28 (d, *J* = 7.1 Hz, 3H), 7.21 (d, *J* = 7.2 Hz, 2H), 6.78 (d, *J* = 8.6 Hz, 1H), 6.66 (d, *J* = 2.4 Hz, 1H), 6.48 (d, *J* = 8.5 Hz, 1H), 5.36 (s, 2H), 5.19 (s, 3H), 4.07–4.00 (m, 2H), 1.08 (t, *J* = 7.1 Hz, 3H); ^{13}C NMR (125 MHz, DMSO-d_6): δ 165.2, 152.3, 146.6, 144.5, 143.6, 140.8, 128.9, 127.9, 126.8, 126.2, 115.1, 114.3, 113.7, 101.2, 64.6, 60.3, 54.5, 14.3; HRMS (ESI): *m/z* calculated for $C_{20}H_{20}ClN_3O_4$ 402.1221 found 402.1218 $[M+H]^+$.

*7.1.1.7. Ethyl 6-((4-chloro-3-methylphenoxy)methyl)-2-oxo-4-(p-tolyl)-1,2,3,4-tetrahydropyrimi dine-5-carboxylate (**6f**).* White solid; yield 92%; mp:189–192 °C; FT-IR (cm^{-1}): 2949, 2822, 1827, 1799, 1370, 747; ^{1}H NMR (500 MHz, DMSO-d_6): δ 9.20 (s, 1H), 7.80 (s, 1H), 7.32 (d, *J* = 8.8 Hz, 1H), 7.13 (s, 4H), 7.02 (d, *J* = 2.5 Hz, 1H), 6.86 (d, *J* = 8.7 Hz, 1H), 5.17 (d, *J* = 4.2 Hz, 2H), 5.01 (d, *J* = 12.0 Hz, 1H), 4.02–3.98 (m, 2H), 2.28 (d, *J* = 7.9 Hz, 6H), 1.06 (t, *J* = 7.1 Hz, 3H); ^{13}C NMR (125 MHz, DMSO-d_6): δ 165.1, 157.1, 152.4, 145.6, 141.6, 137.1, 136.9, 129.9, 129.4, 126.6, 125.6, 118.0, 114.4, 102.2, 64.5, 60.2, 54.2, 21.1, 20.2, 14.3; HRMS (ESI): *m/z* calculated for $C_{22}H_{23}ClN_2O_4$ 415.1425 found 415.1436 $[M+H]^+$.

7.1.1.8. Ethyl 6-((3-chloro-4-fluorophenoxy)methyl)-2-oxo-4-(p-tolyl)-1,2,3,4-tetrahydropyrimi dine-5-carboxylate ***(6g)***. White solid; yield 89%; mp:187–190 °C; FT-IR (cm^{-1}): 2922, 2853, 1822, 1733, 1398, 762; ^{1}H NMR (500 MHz, DMSO-d_6): δ 9.26 (s, 1H), 7.81 (s, 1H), 7.37 (t, J = 9.1 Hz, 1H), 7.27 (d, J = 6.1 Hz, 1H), 7.13 (s, 4H), 7.05–6.98 (m, 1H), 5.18 (t, J = 7.0 Hz, 2H), 5.03 (d, J = 12.0 Hz, 1H), 4.04–3.98 (m, 2H), 2.27 (s, 3H), 1.07 (t, J = 7.1 Hz, 3H); ^{13}C NMR (125 MHz, DMSO-d_6): δ 165.1, 155.0, 155.0, 153.6, 152.4, 151.7, 145.3, 141.5, 137.1, 129.4, 126.6, 120.0, 117.7, 117.5, 117.1, 115.8, 115.7, 102.4, 65.2, 60.3, 54.1, 21.1, 14.3; HRMS (ESI): *m/z* calculated for $C_{21}H_{20}ClFN_2O_4$ 419.1174 found 421.1087 $[M+2]^+$.

7.1.1.9. Ethyl 2-oxo-6-((pyridin-4-yloxy)methyl)-4-(p-tolyl)-1,2,3,4-tetrahydropyrimidine-5-carboxylate ***(6h)***. Yellow solid; yield 87%; mp:190–196 °C; FT-IR (cm^{-1}): 2982, 2843, 1838, 1892, 1489, 742; ^{1}H NMR (500 MHz, DMSO-d_6): δ 7.66 (d, J = 7.5 Hz, 2H), 7.12 (d, J = 7.7 Hz, 3H), 7.01 (d, J = 7.8 Hz, 2H), 6.32 (s, 1H), 6.02 (d, J = 7.5 Hz, 2H), 5.03 (s, 1H), 4.98 (d, J = 13.5 Hz, 1H), 4.88 (d, J = 13.5 Hz, 1H), 4.00–3.90 (m, 2H), 2.24 (s, 3H), 1.07 (t, J = 7.0 Hz, 3H); ^{13}C NMR (125 MHz, DMSO-d_6): δ 177.7, 166.3, 159.5, 145.2, 141.8, 135.8, 128.8, 126.6, 117.2, 58.5, 57.6, 54.8, 21.1, 14.8; HRMS (ESI): *m/z* calculated for $C_{20}H_{21}N_3O_4$ 368.1610 found 368.1622 $[M+H]^+$.

7.1.1.10. Ethyl 2-oxo-6-(((2-oxo-2H-chromen-4-yl)oxy)methyl)-4-(p-tolyl)-1,2,3,4-tetrahydropyrimi dine-5-carboxylate ***(6i)***. White solid; yield 83%; mp:198–202 °C; FT-IR (cm^{-1}): 2922, 2853, 1832, 1793, 1389, 752; ^{1}H NMR (500 MHz, DMSO-d_6): δ 9.57 (s, 1H), 7.87 (d, J = 3.0 Hz, 1H), 7.82 (d, J = 7.9 Hz, 1H), 7.72–7.66 (m, 1H), 7.42 (d, J = 7.6 Hz, 2H), 7.18 (d, J = 7.9 Hz, 4H), 5.98 (s, 1H), 5.37 (d, J = 11.5 Hz, 1H), 5.25 (d, J = 11.6 Hz, 1H), 5.21 (d, J = 3.2 Hz, 1H), 4.05–3.97 (m, 2H), 2.28 (s, 3H), 1.05 (t, J = 7.1 Hz, 3H); ^{13}C NMR (125 MHz, DMSO-d_6): δ 165.1, 155.0, 155.0, 153.6, 152.4, 151.7, 145.3, 141.5, 137.1, 129.4, 126.6, 120.0, 117.7, 117.5, 117.1, 115.8, 115.7, 102.4, 65.2, 60.3, 54.1, 21.1, 14.3; HRMS (ESI): *m/z* calculated for $C_{24}H_{22}N_2O_6$ 435.1556 found 435.1568 $[M+H]^+$.

7.1.1.11. Ethyl 6-((4-chloro-3-methylphenoxy)methyl)-4-(4-chlorophenyl)-2-oxo-1,2,3,4-tetrahydro pyrimidine-5-carboxylate ***(6j)***. White solid; yield 90%; mp:172–176 °C; FT-IR (cm^{-1}): 2983, 2868, 1849, 1765, 1368, 748; ^{1}H NMR (500 MHz, DMSO-d_6): δ 9.31 (s, 1H), 7.88 (s, 1H), 7.42 (d, J = 8.3 Hz, 2H), 7.34 (d, J = 8.7 Hz, 3H), 7.27 (d, J = 8.3 Hz, 2H), 7.02 (s, 1H), 6.87–6.85 (m, 1H), 5.22 (d, J = 3.0 Hz, 1H), 5.18 (d, J = 12.0 HZ, 1H), 5.03 (d, J = 11.9 HZ, 2H), 4.03–3.98 (m, 2H), 2.29 (s, 3H), 1.07 (t, J = 7.1 Hz, 3H); ^{13}C NMR (125 MHz, DMSO-d_6): δ 165.0, 157.1, 152.1, 146.2, 143.4, 136.9, 132.5, 129.9, 128.9, 128.6, 125.7, 118.0, 114.4, 101.6, 64.5, 60.3, 53.9, 20.2, 14.3; HRMS (ESI): *m/z* calculated for $C_{21}H_{20}Cl_2N_2O_4$ 435.0878 found 437.0872 $[M+2]^+$.

7.1.1.12. Ethyl 6-((3-chloro-4-fluorophenoxy)methyl)-4-(4-chlorophenyl)-2-oxo-1,2,3,4-tetrahydro pyrimidine-5-carboxylate ***(6k)***. White solid; yield 90%; mp:170–175 °C; FT-IR (cm^{-1}): 2973, 2853, 1839, 1714, 1398, 748; ^{1}H NMR (500 MHz, DMSO-d_6): δ 9.38 (d, J = 1.2 Hz, 1H), 7.91 (s, 1H), 7.41 (dd, J = 11.3, 4.5 Hz, 2H), 7.39–7.32 (m, 1H), 7.31–7.24 (m, 3H), 7.02 (d, J = 9.1, 1H), 5.21 (d, J = 7.7 Hz, 2H), 5.05 (d, J = 12.0 Hz, 1H), 4.05–3.97 (m, 2H), 1.06 (t, J = 7.1 Hz, 3H); ^{13}C NMR (125 MHz, DMSO-d_6): δ 164.9, 154.9, 153.6, 152.2, 151.7, 145.9, 143.4, 132.5, 128.9, 128.6, 120.0, 117.7, 117.5, 117.1, 115.7, 115.7, 101.7, 65.1, 60.4, 53.9, 14.3; HRMS (ESI): *m/z* calculated for $C_{20}H_{17}Cl_2FN_2O_4$ 439.0628 found 441.0647 $[M+2]^+$.

7.1.1.13. Ethyl 4-(4-chlorophenyl)-2-oxo-6-((pyridin-4-yloxy)methyl)-1,2,3,4-tetrahydropyrim idine-5-carboxylate ***(6l)***. Off white solid, yield 85%; mp:185–189 °C; FT-IR (cm^{-1}): 2972, 2853, 1864, 1710, 1388, 753; ^{1}H NMR (500 MHz, DMSO-d_6): δ 7.82 (s, 1H), 7.70 (d, J = 6.2 Hz, 2H), 7.31 (d, J = 6.4 Hz, 2H), 7.24 (s, 3H), 6.10 (d, J = 6.1 Hz, 2H), 5.21 (s, 1H), 5.11 (d, J = 14.1 Hz, 1H), 4.94 (d, J = 13.9 Hz, 1H), 4.06–4.02 (m, 2H), 1.09 (s, 3H); ^{13}C NMR (125 MHz, DMSO-d_6): δ 177.7, 165.2, 152.6, 145.4, 144.5, 141.1, 128.9, 128.0, 126.8, 117.9, 116.1, 103.1, 60.5, 54.6, 53.0, 14.3; HRMS (ESI): *m/z* calculated for $C_{19}H_{18}ClN_3O_4$ 388.1064 found 388.1079 $[M+H]^+$.

7.1.1.14. Ethyl 4-([1,1′-biphenyl]-4-yl)-2-oxo-6-((pyridin-4-yloxy)methyl)-1,2,3,4-tetrahydro pyrimidine-5-carboxylate ***(6m)***. Yellow solid; yield 87%; mp: 193–197 °C; FT-IR (cm^{-1}): 2976, 2876, 1862, 1712, 1609, 1395, 755; ^{1}H NMR (500 MHz, DMSO-d_6): δ 7.70 (d, J = 7.6 Hz, 3H), 7.67–7.61 (m, 2H), 7.58 (d, J = 8.2 Hz, 2H), 7.45 (t, J = 7.7 Hz, 2H), 7.35 (t, J = 6.8 Hz, 1H), 7.32 (d, J = 8.2 Hz, 2H), 7.22 (s, 1H), 6.08 (d, J = 7.7 Hz, 2H), 5.99 (d, J = 6.5 Hz, 1H), 5.20 (d, J = 2.3 Hz, 1H), 5.11 (d, J = 13.9 Hz, 1H), 4.91 (d, J = 13.9 Hz, 1H), 4.07–3.95 (m, 2H), 1.09 (t, J = 7.1 Hz, 3H); ^{13}C NMR (125 MHz, DMSO-d_6): δ 177.7, 165.5, 146.0, 144.4, 141.3, 140.2, 139.7, 129.3, 127.4, 127.1, 127.0, 117.8, 116.0, 60.2, 54.4, 54.0, 14.5; HRMS (ESI): *m/z* calculated for $C_{25}H_{23}N_3O_4$ 430.1767 found 430.1782 $[M+H]^+$.

7.1.1.15. Ethyl 4-(3-(benzyloxy)phenyl)-2-oxo-6-((pyridin-4-yloxy)methyl)-1,2,3,4-tetrahydro pyrimi dine-5-carboxylate ***(6n)***. Light brown solid; yield 76%; mp: 195–198 °C; FT-IR (cm^{-1}): 2967, 2886, 1878, 1705, 1619, 1385, 765; ^{1}H NMR (500 MHz, DMSO-d_6): δ 9.58 (s, 1H), 7.90 (s, 1H), 7.69 (d, J = 7.5 Hz, 2H), 7.41 (d, J = 7.3 Hz, 4H), 7.33 (t, J = 6.9 Hz, 1H), 7.25 (t, J = 7.9 Hz, 1H), 6.93 (d, J = 8.1 Hz, 1H), 6.88–6.77 (m, 2H), 6.12 (d, J = 7.5 Hz, 2H), 5.20 (d, J = 2.9 Hz, 1H), 5.09 (d, J = 14.2 Hz, 1H), 5.05 (s, 2H), 4.94 (d, J = 14.2 Hz, 1H), 4.06 (t, J = 6.8 Hz, 2H), 1.10 (t, J = 7.0 Hz, 3H); ^{13}C NMR (125 MHz, DMSO-d_6): δ 177.6, 165.2, 158.9, 152.3, 145.9, 144.7, 141.0, 137.4, 130.1, 128.9, 128.3, 128.1, 119.1, 118.0, 114.1, 113.6, 103.4, 69.6, 60.7, 54.4, 52.8, 14.3; HRMS (ESI): *m/z* calculated for $C_{26}H_{25}N_3O_5$ 460.1872 found 460.1869 $[M+H]^+$.

7.1.1.16. Ethyl 4-(3-hydroxyphenyl)-6-((naphthalen-2-yloxy)methyl)-2-oxo-1,2,3,4-tetrahydro pyrimidine-5-carboxylate ***(6o)***. White solid; yield 79%; mp: 188–189 °C; FT-IR (cm^{-1}): 2967, 2881, 1896, 1702, 1609, 1395, 755; ^{1}H NMR (500 MHz, DMSO-d_6): δ 9.43 (s, 1H), 9.28 (s, 1H), 7.83 (d, J = 8.7 Hz, 4H), 7.48 (d, J = 6.9 Hz, 1H), 7.40–7.34 (m, 2H), 7.29 (d, J = 8.9 Hz, 1H), 7.11 (t, J = 7.8 Hz, 1H), 6.76–6.70 (m, 2H), 6.66 (d, J = 8.1 Hz, 1H), 5.34 (d, J = 11.9 Hz, 1H), 5.17 (d, J = 3.4 Hz, 1H), 5.09 (d, J = 11.9 Hz, 1H), 4.06–4.00 (m, 2H), 1.07 (t, J = 7.1 Hz, 3H); ^{13}C NMR (125 MHz, DMSO-d_6): δ 165.2, 157.9, 156.4, 152.5, 145.9, 145.7, 134.5, 129.8, 129.7, 129.2, 128.0, 127.2, 126.9, 124.2, 119.2, 117.3, 114.9, 113.7, 107.5, 102.2, 64.4, 60.3, 54.4, 14.3; HRMS (ESI): *m/z* calculated for $C_{24}H_{22}N_2O_5$ 419.1607 found 419.1610 $[M+H]^+$.

7.1.1.17. Ethyl 6-((3,5-dimethoxyphenoxy)methyl)-4-(3-hydroxyphenyl)-2-oxo-1,2,3,4-tetrahydro pyrimidine-5-carboxylate ***(6p)***. Off white solid; yield 73%; mp:187–191 °C; FT-IR (cm^{-1}): 2931, 2611, 1869, 1739, 1738, 1675, 1385, 795; ^{1}H NMR (500 MHz, DMSO-d_6): δ 9.41 (s, 1H), 9.16 (s, 1H), 7.82–7.77 (m, 1H), 7.10 (t, J = 7.8 Hz, 1H), 6.71–6.64 (m, 3H), 6.18 (d, J = 2.1 Hz, 2H), 6.13 (t, J = 2.1 Hz, 1H), 5.19 (d, J = 12.0 Hz, 1H), 5.13 (d, J = 3.3 Hz, 1H), 4.92 (d, J = 12.1 Hz, 1H), 4.05–3.99 (m, 2H), 3.70 (s, 6H), 1.09 (t, J = 7.1 Hz, 3H); ^{13}C NMR (125 MHz, DMSO-d_6): δ 165.2, 161.6, 160.2, 157.9, 152.4, 145.9, 145.7, 129.8, 117.2, 114.9, 113.7, 102.1, 94.0, 64.3, 60.3, 55.6, 54.3, 14.3; .HRMS (ESI): *m/z* calculated for $C_{22}H_{24}N_2O_7$ 429.1662 found 431.1678 $[M+2]^+$.

7.1.1.18. Ethyl 6-((2-amino-4-chlorophenoxy)methyl)-2-oxo-4-(thiophen-2-yl)-1,2,3,4-tetrahydro pyrimidine-5-carboxylate ***(6q)***. Off white solid; yield 73%; mp:189–193 °C; FT-IR (cm^{-1}): 2986, 2611, 1879, 1563, 1384, 1175, 785; ^{1}H NMR (500 MHz, DMSO-d_6): δ 9.44 (s, 1H), 8.02 (s, 1H), 7.39 (d, J = 5.0 Hz, 1H), 6.97 –6.92 (m, 1H), 6.90 (d, J = 3.0 Hz, 1H), 6.76 (d, J = 8.6 Hz, 1H), 6.65 (d, J = 2.2 Hz, 1H), 6.48 (dd,

J = 8.5, 2.2 Hz, 1H), 5.47 (d, J = 3.4 Hz, 1H), 5.34 (s, 2H), 5.24 (d, J = 13.6 Hz, 1H), 5.05 (d, J = 13.6 Hz, 1H), 4.13–4.09 (m, 2H), 1.16 (t, J = 7.1 Hz, 3H); ^{13}C NMR (125 MHz, DMSO-d_6): δ 164.9, 152.4, 148.3, 146.8, 143.7, 140.7, 127.2, 126.2, 125.4, 124.3, 115.1, 114.1, 113.7, 101.5, 64.5, 60.4, 49.8, 14.4; HRMS (ESI): *m/z* calculated for $C_{18}H_{18}ClN_3O_4S$ 408.0785 found 408.0768 $[M+H]^+$.

*7.1.1.19. Ethyl 6-((3,5-dimethoxyphenoxy)methyl)-2-oxo-4-(thiophen-2-yl)-1,2,3,4-tetrahydro pyrimidine-5-carboxylate (**6r**)*. Light brown solid; yield 78%; mp:188–191 °C; FT-IR (cm^{-1}): 2898, 2609, 1859, 1563, 1394, 1275, 785; ^{1}H NMR (500 MHz, DMSO-d_6): δ 9.34 (s, 1H), 8.02 (s, 1H), 7.40 (d, J = 5.0 Hz, 1H), 6.96 (d, J = 4.9 Hz, 1H), 6.93 (d, J = 3.3 Hz, 1H), 6.18 (d, J = 2.1 Hz, 2H), 6.13 (d, J = 2.0 Hz, 1H), 5.49 (d, J = 3.5 Hz, 1H), 5.21 (d, J = 12.2 Hz, 1H), 4.90 (d, J = 12.2 Hz, 1H), 4.10–4.08 (m, 2H), 3.70 (s, 6H), 1.14 (t, J = 7.1 Hz, 3H); ^{13}C NMR (125 MHz, DMSO-d_6): δ 164.8, 161.5, 160.2, 152.5, 148.2, 146.2, 127.2, 125.4, 124.3, 102.2, 93.9, 93.9, 64.1, 60.5, 55.6, 49.9, 14.4; HRMS (ESI): *m/z* calculated for $C_{20}H_{22}N_2O_6S$ 419.1277 found 419.1261 $[M+H]^+$.

*7.1.1.20. Ethyl 6-((3,5-dimethoxyphenoxy)methyl)-4-(furan-2-yl)-2-oxo-1,2,3,4-tetrahydropyrimid ine-5-carboxylate (**6s**)*. Light brown solid; yield 69%; mp:183–187 °C; FT-IR (cm^{-1}): 2920, 2651, 1851, 1556, 1389, 1285, 760; ^{1}H NMR (500 MHz, DMSO-d_6): δ 9.25 (s, 1H), 7.88 (s, 1H), 7.58 (d, J = 1.0 Hz, 1H), 6.38 (d J = 3.1 Hz, 1H), 6.19 (d, J = 2.1 Hz, 2H), 6.16–6.10 (m, 2H), 5.29 (d, J = 3.4 Hz, 1H), 5.22 (d, J = 12.2 Hz, 1H), 4.93 (d, J = 12.2 Hz, 1H), 4.08–4.04 (m, 2H), 3.71 (s, 6H), 1.12 (t, J = 7.1 Hz, 3H); ^{13}C NMR (125 MHz, DMSO-d_6): δ 164.8, 161.5, 160.2, 155.6, 152.6, 147.0, 142.8, 110.8, 106.1, 99.4, 94.0, 64.1, 60.3, 55.6, 48.2, 14.4; HRMS (ESI): *m/z* calculated for $C_{20}H_{22}N_2O_7$ 403.1505 found 403.1520 $[M+H]^+$.

*7.1.1.21. Ethyl 6-((2-(2-bromoacrylamido)-4-chlorophenoxy)methyl)-2-oxo-4-(thiophen-2-yl)-1,2,3,4-tetrahydropyrimidine-5-carboxylate (**10a**)*. White solid; yield 88%; mp: 192–196 °C; FT-IR (cm^{-1}): 3346, 3119, 2986, 1689, 1654, 1527, 1203, 875; ^{1}H NMR (500 MHz, DMSO-d_6): δ 9.61 (s, 1H), 9.49 (s, 1H), 8.14–7.95 (m, 2H), 7.41 (d, J = 4.9 Hz, 1H), 7.23 (d, J = 8.8 Hz, 1H), 7.07 (d, J = 8.9 Hz, 1H), 7.03–6.91 (m, 2H), 6.87 (d, J = 2.6 Hz, 1H), 6.35 (d, J = 2.6 Hz, 1H), 5.51 (d, J = 3.4 Hz, 1H), 5.29 (d, J = 13.3 Hz, 2H), 4.11–4.07 (m, 2H), 1.16 (t, J = 7.1 Hz, 3H); ^{13}C NMR (125 MHz, DMSO-d_6): δ 164.8, 160.3, 152.4, 148.1, 147.6, 145.8, 128.3, 128.2, 127.2, 125.5, 125.4, 124.4, 123.7, 121.8, 114.0, 102.2, 65.0, 60.6, 49.9, 14.4; HRMS (ESI): *m/z* calculated for $C_{21}H_{19}BrClN_3O_5S$ 539.9996 found 541.9971 $[M+2]^+$.

*7.1.1.22. Ethyl 6-((2-(2-bromoacrylamido)-4-chlorophenoxy)methyl)-4-(furan-2-yl)-2-oxo-1,2,3,4-tetrahydropyrimidine-5-carboxylate (**10b**)*. White solid; yield 95%; mp: 190–195 °C; FT-IR (cm^{-1}): 3369, 3285, 2981, 1695, 1656, 1635, 1253, 831; ^{1}H NMR (500 MHz, DMSO-d_6): δ 9.63 (s, 1H), 9.41 (s, 1H), 8.02 (d, J = 2.6 Hz, 1H), 7.92 (s, 1H), 7.58 (d, J = 5.9 Hz, 1H), 7.25 (d, J = 8.8 Hz, 1H), 7.08 (d, J = 8.9 Hz, 1H), 6.87 (d, J = 2.6 Hz, 1H), 6.39 (d, J = 3.1 Hz, 1H), 6.35 (d, J = 2.6 Hz, 1H), 6.17 (d, J = 3.1 Hz, 1H), 5.36 (d, J = 13.3 Hz, 1H), 5.29 (d, J = 3.4 Hz, 1H), 5.24 (d, J = 13.3 Hz, 1H), 4.09–4.06 (m, 2H), 1.13 (t, J = 7.1 Hz, 3H); ^{13}C NMR (125 MHz, DMSO-d_6): δ 164.8, 160.3, 155.6, 152.6, 147.7, 146.7, 142.9, 128.3, 128.2, 125.5, 125.3, 123.7, 121.9, 114.1, 110.9, 106.2, 99.2, 65.0, 60.4, 48.2, 14.4; HRMS (ESI): *m/z* calculated for $C_{21}H_{19}BrClN_3O_6$ 524.0224 found 526.0223 $[M+2]^+$.

*7.1.1.23. Ethyl 6-((2-(2-bromoacrylamido)-4-chlorophenoxy)methyl)-2-oxo-4-phenyl-1,2,3,4-tetra- hydropyrimidine-5-carboxylate (**10c**)*. White solid; yield 95%; mp: 198–202 °C; FT-IR (cm^{-1}): 3367, 3151, 2891, 1692, 1675, 1643, 1425, 955; ^{1}H NMR (500 MHz, DMSO-d_6): δ 9.63 (d, J = 9.4 Hz, 1H), 9.38 (d, J = 9.4 Hz, 1H), 8.04 (d, J = 9.1 Hz, 1H), 7.88 (d, J = 7.2 Hz, 1H), 7.29 (d, J = 6.9 Hz, 6H), 7.09 (d, J = 8.7 Hz, 1H), 6.88 (d, J = 8.2 Hz, 1H), 6.35 (d, J = 7.2 Hz, 1H), 5.32 (d, J = 7.8 Hz, 2H), 5.23 (d, J = 8.4 Hz, 1H), 4.07–3.99 (m, 2H), 1.08 (t, J = 14.1, 7.0 Hz, 3H); ^{13}C NMR (125 MHz, DMSO-d_6): δ 165.1, 160.3, 152.3, 147.6, 145.6, 144.5, 128.9, 128.4, 128.3, 128.0, 126.8, 125.4, 121.8, 114.1, 102.0, 65.2, 60.4, 54.6, 14.3; HRMS (ESI): *m/z* calculated for $C_{23}H_{21}BrClN_3O_5$ 534.0431 found 536.0420 $[M+2]^+$.

*7.1.1.24. Ethyl 6-((2-(2-bromoacrylamido)-4-chlorophenoxy)methyl)-4-(4-chlorophenyl)-2-oxo-1,2, 3, 4-tetrahydropyrimidine-5-carboxylate (**10d**)*. White solid; yield 89%; mp: 196–199 °C; FT-IR (cm^{-1}): 3368, 3112, 2889, 1698, 1675, 1638, 1412, 890; ^{1}H NMR (500 MHz, DMSO-d_6): δ 9.61 (s, 1H), 9.40 (s, 1H), 8.02 (d, J = 2.5 Hz, 1H), 7.91 (s, 1H), 7.40 (d, J = 8.4 Hz, 2H), 7.25 (d, J = 5.4 Hz, 3H), 7.08 (d, J = 8.9 Hz, 1H), 6.87 (d, J = 2.5 Hz, 1H), 6.35 (d, J = 2.5 Hz, 1H), 5.31 (s, 2H), 5.23 (d, J = 3.1 Hz, 1H), 4.04–3.99 (m, 2H), 1.08 (t, J = 7.1 Hz, 3H); ^{13}C NMR (125 MHz, DMSO-d_6): δ 165.0, 160.3, 152.1, 147.6, 146.0, 143.4, 132.5, 128.9, 128.7, 128.3, 125.5, 123.7, 121.8, 114.2, 101.5, 65.2, 60.5, 54.0, 14.3; HRMS (ESI): *m/z* calculated for $C_{23}H_{20}BrCl_2N_3O_5$ 568.0042 found 570.0033 $[M+2]^+$.

*7.1.1.25. Ethyl 6-((2-(2-bromoacrylamido)-4-chlorophenoxy)methyl)-4-(4-bromophenyl)-2-oxo-1,2,3,4-tetrahydropyrimidine-5-carboxylate (**10e**)*. White solid; yield 82%; mp: 198–205 °C; FT-IR (cm^{-1}): 3366, 3207, 2926, 1696, 1685, 1587, 1253, 875; ^{1}H NMR (500 MHz, DMSO-d_6): δ 9.59 (s, 1H), 9.38 (s, 1H), 8.02 (d, J = 2.5 Hz, 1H), 7.91 (s, 1H), 7.38 (d, J = 8.2 Hz, 2H), 7.27 (d, J = 6.4 Hz, 3H), 7.08 (d, J = 7.9 Hz, 1H), 6.86 (d, J = 3.5 Hz, 1H), 6.33 (d, J = 3.5 Hz, 1H), 5.29 (s, 2H), 5.23 (d, J = 3.3 Hz, 1H), 4.04–3.99 (m, 2H), 1.08 (t, J = 7.1 Hz, 3H); ^{13}C NMR (125 MHz, DMSO-d_6): δ 164.8, 160.3, 155.6, 152.6, 147.7, 146.7, 142.9, 128.3, 128.2, 125.5, 125.3, 123.7, 121.9, 114.1, 110.9, 106.2, 99.2, 65.0, 60.4, 48.2, 14.4; HRMS (ESI): *m/z* calculated for $C_{23}H_{20}Br_2ClN_3O_5$ 611.9536 found 613.9519 $[M+2]^+$.

*7.1.1.26. Ethyl 6-((4-(2-bromoacrylamido)phenoxy)methyl)-2-oxo-4-(p-tolyl)-1,2,3,4-tetrahydro pyrimidine-5-carboxylate (**10f**)*. White solid; yield 95%; mp: 199–202 °C; FT-IR (cm^{-1}): 3274, 2967, 2881, 1732, 1702, 1609, 1495, 755; ^{1}H NMR (500 MHz, DMSO-d_6): δ 10.16 (s, 1H), 9.18 (d, J = 1.4 Hz, 1H), 7.80 (s, 1H), 7.57 (d, J = 9.0 Hz, 2H), 7.14 (s, 4H), 7.02–6.96 (m, 2H), 6.73 (d, J = 3.0 Hz, 1H), 6.28 (d, J = 3.0 Hz, 1H), 5.18 (d, J = 9.7 Hz, 2H), 4.99 (d, J = 12.0 Hz, 1H), 4.01–3.99 (m, 2H), 2.27 (s, 3H), 1.06 (t, J = 7.1 Hz, 3H); ^{13}C NMR (125 MHz, DMSO-d_6): δ 165.1, 161.1, 155.0, 152.4, 145.9, 141.6, 137.1, 132.3, 129.4, 126.6, 125.9, 125.6, 122.4, 115.3, 102.1, 64.5, 60.2, 54.2, 21.1, 14.3; HRMS (ESI): *m/z* calculated for $C_{24}H_{24}BrN_3O_5$ 514.0978 found 516.0968 $[M+2]^+$.

*7.1.1.27. Ethyl 4-([1,1′-biphenyl]-4-yl)-6-((4-(2-bromoacrylamido) phenoxy)methyl)-2-oxo-1,2,3,4-tetrahydropyrimidine-5-carboxylate (**10g**)*. White solid; yield 78%; mp: 200–206 °C; FT-IR (cm^{-1}): 3364, 3151, 2881, 1685, 1646, 1527, 1418, 813; ^{1}H NMR (500 MHz, DMSO-d_6): δ 9.61 (s, 1H), 9.40 (s, 1H), 8.02 (d, J = 2.5 Hz, 1H), 7.91 (s, 1H), 7.40 (d, J = 8.4 Hz, 2H), 7.25 (d, J = 13.6 Hz, 3H), 7.08 (d, J = 8.9 Hz, 1H), 6.87 (d, J = 2.5 Hz, 1H), 6.35 (d, J = 2.5 Hz, 1H), 5.31 (s, 2H), 5.23 (d, J = 3.1 Hz, 1H), 4.11 (d, J = 7.0 Hz, 2H), 1.08 (t, J = 7.1 Hz, 3H); ^{13}C NMR (125 MHz, DMSO-d_6): δ 165.2, 161.2, 154.9, 152.4, 146.1, 143.5, 140.1, 139.9, 129.4, 127.4, 127.2, 127.0, 126.1, 122.5, 115.4, 102.0, 64.5, 60.4, 54.1, 14.3; HRMS (ESI): *m/z* calculated for $C_{29}H_{26}BrN_3O_5$ 576.1134 found 578.1136 $[M+2]^+$.

7.2. Pharmacology

7.2.1. Cell culture

Cancer cell lines such as colon (HCT-116 and HCT-15, HT-29), Prostate (DU 145) breast (MCF-7, MDA MB-231) were maintained in Roswell Park Memorial Institute (RPMI) media while normal lung fibroblasts cell line (HFL-1) were maintained in F12k medium

supplemented with 10% fetal bovine serum (FBS) stabilized with 1% antibiotic-antimycotic solution (Sigma) cells were maintained in 5% CO_2 and 98% relative humidity at 37 °C in incubator. When the cells reached up to 80–90% of confluency, they were sub-cultured using 0.25% trypsin/1 mM EDTA solution for further passage. The compounds were dissolved in DMSO to prepare the stock solution of 10 mM. Further dilutions were made accordingly with respective media to get required concentration (0–50 μM).

7.2.2. Evaluation of in vitro cytotoxic effects

It is a colorimetric assay that measures the reduction of MTT (3-(4,5-dimethyl thiazol- 2-yl)-2,5-diphenyl tetrazolium bromide) to insoluble formazon by mitochondrial succinate dehydrogenase enzyme. Since reduction of MTT can only happen in metabolically active cells, the level of activity is the measure of the viability of the cells [37]. Briefly, cells were seeded in 96-well plates at a density of 1000 to 4000 cells per well in 100 μL of complete medium and allowed to grow overnight for attachment onto the wells. Then the cells were treated with various concentrations (0–50 μM) of the compounds for a period of 72 h. For cell growth inhibition analysis after 24 h of cell seeding, before treatment (day 0), absorbance was measured by adding MTT in few wells. After 72 h incubation, 100 μL of MTT (0.5 mg/ml) was added and incubated at 37 °C for 4 h. Then MTT reagent was aspirated and the formazan crystals formed were dissolved by the addition of 200 μL of DMSO for 20 min. at 37 °C. The formazon product quantity was measured by using a spectrophotometric microtiter plate reader (Spectra Max, M4 Molecular devices, USA) at 570 nm wavelength. The day 0 absorbance was subtracted from the 72 h plates for determining growth inhibition and data were plotted as a percentage of untreated control.

*7.2.3. Effect of **10f** on tubulin polymerization inhibition*

Tubulin polymerization kit was procured from Cytoskeleton, Inc. (BK011). To study the effect of compound **10f**, fluorescence based *in vitro* tubulin polymerization assay was performed following the manufacturer's protocol. The reaction mixture having porcine brain tissue (2 mg/mL) in 80 mM PIPES at pH 6.9, 2.0 mM $MgCl_2$, 0.5 mM EGTA, 1.0 mM GTP and glycerol in the presence and absence of test compound **10f** (final concentration of 10 mM) was prepared and added to each well of 96-well plate. Tubulin polymerization was followed by a time dependent increase in fluorescence due to the insertion of a fluorescence reporter into microtubules as polymerization takes place. Spectramax M4 Multi mode Micro plate Detection System was used to measure Fluorescence emission at 440 nm (excitation wavelength is 360 nm). podophyllotoxin was used as positive control in the assay at 5 μM final concentration. The IC_{50} value was calculated from the drug concentration required for inhibiting 50% of tubulin assembly compared to control. Another compound namely, Paclitaxel will stabilize the microtubule. The IC_{50} value was calculated from the drug concentration required for inhibiting 50% of tubulin assembly compared to control.

7.2.4. Molecular docking

The crystal co-ordinates of α,β-tubulin subunits were retrieved from the protein data bank (PDB ID: 1SA0). The 3D structure of compound **10f** was drawn on Maestro Molecule Builder of Schrödinger. The molecule was optimized using OPLS_2005 force field in LigPrep module of Schrödinger. Docking procedure was performed according to the standard protocol implemented in maestro software, version 9.9 and the compound **10f** was docked into the α,β -tubulin interphase. The ligand-protein complex was analyzed for interactions and 3D pose of most active compound **10f** was imaged using Schrödinger.

7.2.5. Analysis of cell cycle effect

Flow cytometric analysis (FACS) was performed to calculate the distribution of the cell population in various cell cycle phases. In general the novel compounds exert their cytotoxic or growth inhibitory effect by arresting the specific checkpoint in cell cycle. Here MCF-7 cancer cells were incubated with compound **10f** at 0.5 μM for 48 h. Untreated and treated cells were harvested, washed and fixed overnight in 70% ethanol in PBS at −20 °C. Fixed cells were pelleted and stained with cell cycle analysis reagent propidium iodide (50 μg/ml) with RNase A for 20 min. at 37 °C in dark according to the manufacturer instructions and about 10,000 events were acquired and analyzed on a flow cytometer BD FACSVerseTM (BD Biosciences, USA).

7.2.6. Identification of apoptotic cells

Morphological changes in nucleus were observed through DAPI staining. After treatment with compound **10f** for 72 h, breast cancer cell line MCF-7 cells were washed with PBS and permeabilized with 0.1% Tween 20 for 10 min followed by staining with 1 μM DAPI. Control and treated cells were observed with fluorescence microscope with excitation at 359 nm and emission at 461 nm using DAPI filter at 200x magnification.

7.2.7. Detection of morphology during apoptosis induction

MCF-7 cells were plated at a concentration of 1×10^6 cells/ml and treated with different concentrations of compound **10f** and the plates were incubated for 72 h. 10 μL of fluorescent dyes containing Acridine Orange (AO) and Ethidium Bromide (EB) were added into each well in equal volumes (10 μg/ml) respectively then the cells were visualized immediately under fluorescence microscope (Nikon, Inc. Japan) with excitation (488 nm) and emission (550 nm) at 200X magnification.

7.2.8. Quantification of apoptotic cells

It was performed by the method given by Rieger et al [38] with slight modifications. Briefly, 1x 10^5 cells were seeded in a 12-well plate and treated with different concentration of compound **10f** for 72 h. Then Untreated and treated cells were harvested and the cells were processed with Annexin V-FITC and Propidium Iodide (PI) staining (BioLegend) according to the manufacturer's instructions. Further, flow cytometric analysis was performed using a flow cytometer (BD FACSVerseTM, USA). Apoptosis and necrosis were analyzed with quadrant statistics on propidium iodide-negative cells, fluorescein positive cells and propidium iodide (PI)-positive cells, respectively.

7.2.9. Effect on mitochondrial membrane potential

Measurement of mitochondrial membrane potential, MCF-7 cells (1x10^6 cells/ml) were seeded in 12 well plates and allowed to adhere for overnight. The cells were incubated with compound **10f** at 0.25, 0.5, and 2 μM concentrations for 72 h. Cells were collected and washed with PBS and resuspended in solution of JC-1 (1 μM) and incubated for 30 min in incubator at 37 °C. The cells were washed twice with PBS and analysed by flow cytometer (BD FACSVerse™, USA).

*7.2.10. Effect of **10f** on intracellular ROS generation*

DCFDA staining was performed to determine the reactive oxygen species (ROS) levels as per reported method [39] with slight modifications. For this experiment, MCF-7 cells were plated at cell density of 3.5x10^5 cells/well into 12-well plates in Roswell Park Memorial Institute (RPMI) supplemented with 10% FBS. Then the cells were treated with the compound **10f** at various concentrations for 72 h. Then the DCFDA reagent was added at 10 μM concentration for 15 min and the fluorescent intensity was obtained using fluorescent spectrophotometer (Hitachi F7000). The fluorescence readings were taken thrice to eliminate errors.

Declaration of Competing Interest

The authors declare no conflicts of interest.

Acknowledgements

SS and RT are thankful to DoP, Ministry of Chemicals & Fertilizers, Govt. of India, New Delhi, for the award of NIPER fellowship. Dr. N. Shankaraiah thankful to SERB, DST, Govt. of India for the start-up grant (YSS-2015-001709).

Appendix A. Supplementary material

Supplementary data to this article can be found online at https://doi.org/10.1016/j.bioorg.2019.103317.

References

[1] a) https://www.cancer.gov/about-cancer/understanding/statistics.
b) R.L. Siegel, K.D. Miller, A. Jemal, Cancer statistics, CA Cancer J. Clin. 69 (2019) (2019) 7–34
[2] https://www.medicalnewstoday.com/articles/322923.php.
[3] a) M.M. Gottesman, O. Lavi, M.D. Hall, J.P. Gillet, Toward a better understanding of the complexity of cancer drug resistance, Annu. Rev. Pharmacol. Toxicol. 56 (2016) 85–102;
b) R.W. Robey, K.M. Pluchino, M.D. Hall, A.T. Fojo, S.E. Bates, M.M. Gottesman, Revisiting the role of ABC transporters in multidrug-resistant cancer, Nat. Rev. Cancer. 18 (2018) 452–464;
c) S. Nekkanti, O. Ommi , P.S.S. Lakshmi, N. Shankaraiah, Diverse targeted approaches to battle multidrug resistance in cancer, http://doi.org/10.2174/0929867325666180410110729.
[4] a) B. Kumar, R. Kumar, I. Skvortsova, V. Kumar, Mechanisms of tubulin binding ligands to target cancer cells: updates on their therapeutic potential and clinical trials, Curr. Cancer Drug Targets. 17 (2017) 357–375;
b) R. Kaur, G. Kaur, R.K. Gill, R. Soni, J. Bariwal, Recent developments in tubulin polymerization inhibitors: An overview, Eur. J. Med. Chem. 87 (2014) 89–124;
c) M.A. Jordan, L. Wilson, Microtubules as a target for anticancer drugs, Nat. Rev. Cancer. 4 (2004) 253–265;
d) R.O. Carlson, New tubulin targeting agents currently in clinical development, Expert Opin. Invest. Drugs 17 (2008) 707–722;
d) J. Seligmann, C. Twelves, Tubulin: an example of targeted chemotherapy, Future Med. Chem. 5 (2013) 339–352.
[5] a) X.X. Wu, Q.H. Wang, W. Li, Recent advances in heterocyclic tubulin inhibitors targeting the colchicine binding site, Anti-Cancer Agent. Me 16 (2016) 1325–1338;
b) D.J. Newman, G.M. Cragg, Natural products as sources of new drugs from 1981 to 2014, J. Nat. Prod 79 (2016) 629–661;
c) M. Dong, F. Liu, H. Zhou, S. Zhai, B. Yan, Novel natural product-and privileged scaffold-based tubulin inhibitors targeting the colchicine binding site, Molecules 21 (2016) 1375;
d) T.L. Simmons, E. Andrianasolo, K. McPhail, P. Flatt, W.H. Gerwick, Marine natural products as anticancer drugs, Mol. Cancer Ther. 4 (2005) 333–342.
[6] a) M. Kavallaris, Microtubules and resistance to tubulin-binding agents, Nat. Rev. Cancer 10 (2010) 194–204;
b) K.E. Arnst, Y. Wang, D.J. Hwang, Y. Xue, T. Costello, D. Hamilton, Q. Chen, J. Yang, F. Park, J.T. Dalton, D.D. Miller, W. Li, A. Potent, Metabolically stable tubulin inhibitor targets the colchicine binding site and overcomes taxane resistance, Cancer Res. 78 (2018) 265–277;
c) E.A. Perez, Microtubule inhibitors: differentiating tubulin-inhibiting agents based on mechanisms of action, clinical activity, and resistance, Mol. Canc. Therapeut. 8 (2009) 2086–2095.
[7] C. Kanthou, G.M. Tozer, Microtubule depolymerizing vascular disrupting agents: novel therapeutic agents for oncology and other pathologies, Int. J. Exp. Pathol. 90 (2009) 284–294.
[8] R. Kaur, P. Kaur, S. Sharma, G. Singha, S. Mehndiratta, P.M.S. Bedia, K. Nepalia, Anti-cancer pyrimidines in diverse scaffolds: a review of patent literature, Recent Patents Anti-Cancer Drug Discov. 10 (2015) 23–71.
[9] a) R. Kaur, S. Chaudhary, K. Kumar, M.K. Gupta, R.K. Rawal, Recent synthetic and medicinal perspectives of dihydropyrimidinones: A review, Eur. J. Med. Chem. 132 (2017) 108–134;
b) X. Qian, A.A. Wolff, G. Bergnes, Progress on mitotic kinesin inhibitors as anticancer therapeutics, Annu. Rep. Med. Chem. 41 (2006) 263–274;
c) B.S. Holla, B.S. Rao, B. Sarojini, P. Akberali, One pot synthesis of thiazolo dihydro pyrimidinones and evaluation of their anticancer activity, Eur. J. Med. Chem. 39 (2004) 777–783;
d) E.D. Edstrom, Y. Wei, Synthesis of a novel pyrrolo[2,3-d]pyrimidine alkaloid, rigidin, J. Org. Chem. 58 (1993) 403–407.
[10] a) K.S. Atwal, B.N. Swanson, S.E. Unger, D.M. Floyd, S. Moreland, A. Hedberg, B.C. O'Reilly, Dihydropyrimidine calcium channel blockers. 3. 3-Carbamoyl-4- aryl-1, 2, 3, 4-tetrahydro-6-methyl-5-pyrimidine carboxylic acid esters as orally effective antihypertensive agents, J. Med. Chem. 34 (1991) 806–811;
b) O. Alam, S.A. Khan, N. Siddiqui, W. Ahsan, S.P. Verma, S.J. Gilani, Antihypertensive activity of newer 1, 4-dihydro-5-pyrimidine carboxamides: synthesis and pharmacological evaluation, Eur. J. Med. Chem. 45 (2010) 5113–5119.
[11] a) S.M. Sondhi, N. Singh, M. Johar, A. Kumar, Synthesis, anti-inflammatory and analgesic activities evaluation of some mono, bi and tricyclic pyrimidine derivatives, Bioorg. Med. Chem. 13 (2005) 6158–6166;
b) S.A. Said, A.E.G.E. Amr, N.M. Sabry, M.M. Abdalla, Analgesic, anticonvulsant and anti-inflammatory activities of some synthesized benzodiazipine, triazolopyrimidine and bis-imide derivatives, Eur. J. Med. Chem. 44 (2009) 4787–4792.
[12] E. Rajanarendar, M.N. Reddy, K.R. Murthy, K.G. Reddy, S. Raju, M. Srinivas, B. Praveen, M.S. Rao, Synthesis, antimicrobial, and mosquito larvicidal activity of 1-Aryl-4-methyl-3, 6-bis-(5-methylisoxazol-3-yl)-2-thioxo-2, 3, 6, 10*b*-tetrahydro-1*H*-pyrimido [5, 4-*c*] quinolin-5-ones, Bioorg. Med. Chem. Lett. 20 (2010) 6052–6055.
[13] a) G. Lauro, M. Strocchia, S. Terracciano, I. Bruno, K. Fischer, C. Pergola, O. Werz, R. Riccio, G. Bifulco, Exploration of the dihydropyrimidine scaffold for the development of new potential anti-inflammatory agents blocking prostaglandin E_2 synthase-1 enzyme (mPGES-1), Eur. J. Med. Chem. 80 (2014) 407–415.
[14] a) A.R. Trivedi, V.R. Bhuva, B.H. Dholariya, D.K. Dodiya, V.B. Kataria, V.H. Shah, Novel dihydropyrimidines as a potential new class of antitubercular agents, Bioorg. Med. Chem. Lett. 20 (2010) 6100–6102;
b) R.K. Yadlapalli, O. Chourasia, K. Vemuri, M. Sritharan, R.S. Perali, Synthesis and in vitro anticancer and antitubercular activity of diarylpyrazole ligated dihydropyrimidines possessing lipophilic carbamoyl group, Bioorg. Med. Chem. Lett. 22 (2012) 2708–2711.
[15] a) B.N. Naidu, M.E. Sorenson, M. Patel, Y. Ueda, J. Banville, F. Beaulieu, S. Bollini, I.B. Dicker, H. Higley, Z. Lin, Synthesis and evaluation of C2-carbon-linked heterocyclic-5-hydroxy-6-oxo-dihydropyrimidine-4-carboxamides as HIV-1 integrase inhibitors, Bioorg. Med. Chem. Lett. 25 (2015) 717–720;
b) M. Dragunow, Adenosine receptor antagonism accounts for the seizure prolonging effects of aminophylline, Pharmacol. Biochem. Behav. 36 (1990) 751–755;
c) R.H. Tale, A.H. Rodge, G.D. Hatnapure, A.P. Keche, The novel 3, 4-dihydropyrimidin-2(1H)-one urea derivatives of N-aryl urea: synthesis, anti-inflammatory, antibacterial and antifungal activity evaluation, Bioorg. Med. Chem. Lett. 21 (2011) 4648–4651.
[16] a) F.A.F. Ragab, S.M. Abou-Seri, S.A. Abdel-Aziz, A.M. Alfayomy, M. Aboelmagd, Design, synthesis and anticancer activity of new monastrol analogues bearing 1,3,4-oxadiazole moiety, Eur. J. Med. Chem. 138 (2017) 140–151;
b) H.Y.K. Kaan, V. Ulaganathan, O. Rath, H. Prokopco, D. Dallinger, C.O. Kappe, F. Kozielski, Structural Basis for Inhibition of Eg5 by Dihydropyrimidines: Stereoselectivity of Antimitotic Inhibitors Enastron, Dimethylenastron and Fluorastrol, J. Med. Chem. 53 (2010) 5676–5683.
[17] R. Pellicciari, P. Liscio, N. Giacchè, F. De Franco, A. Carotti, J. Robertson, L. Cialabrini, E. Katsyuba, N. Raffaelli, J. Auwerx, α-Amino-β-carboxymuconate-ε-semialdehyde Decarboxylase (ACMSD) inhibitors as novel modulators of *de novo* Nicotinamide Adenine Dinucleotide (NAD^+) Biosynthesis, J. Med. Chem. 61 (2018) 745–759.
[18] T.U. Mayer, T.M. Kapoor, S.J. Haggarty, R.W. King, S.I. Schreiber, T.J. Mitchison, Small molecule inhibitor of mitotic spindle bipolarity identified in a phenotype-based screen, Science 268 (1999) 971–974.
[19] C.J. Burns, E. Fantino, I.D. Phillips, S. Su, M.F. Harte, P.E. Bukczynska, M. Frazzetto, M. Joffe, I. Kruszelnicki, B. Wang, Y. Wang, N. Wilson, R.J. Dilley, S.S. Wan, S.A. Charman, D.M. Shackleford, R. Fida, C. Malcontenti-Wilson, A.F. Wilks, CYT997: a novel orally active tubulin polymerization inhibitor with potent cytotoxic and vascular disrupting activity *in vitro* and *in vivo*, Mol Cancer Ther. 8 (2009) 3036–3045.
[20] a) M.H. Potashman, M.E. Duggan, Covalent Modifiers: An orthogonal approach to drug design, J. Med. Chem. 52 (2009) 1231–1246;
b) R.A. Bauer, Covalent inhibitors in drug discovery: from accidental discoveries to avoided liabilities and designed therapies, Drug Discov. Today 20 (2015) 1061–1073;
c) J. Singh, R.C. Petter, T.A. Baillie, A. Whitty, The resurgence of covalent drugs, Nat. Rev. Drug Discov. 10 (2011) 307–317;
d) D.S. Johnson, E. Weerapana, B.F. Cravatt, Strategies for discovering and derisking covalent, irreversible enzyme inhibitors, Future Med. Chem. 2 (2010) 949–964.
[21] a) R. Romagnoli, P.G. Baraldi, M.A. Iaconinoto, M.D. Carrion, M.A. Tabrizi, R. Gambari, M. Borgatti, J. Heilmann, Synthesis and biological activity of alpha-bromoacryloyl lexitropsin conjugates, Eur. J. Med. Chem. 40 (2005) 1123–1128;
b) R. Romagnoli, P.G. Baraldi, M.K. Salvador, M. Chayah, M.E. Camacho, F. Prencipe, E. Hamel, F. Consolaro, G. Basso, G. Viola, Design, synthesis and biological evaluation of arylcinnamide hybrid derivatives as novel anticancer agents, Eur. J. Med. Chem. 81 (2014) 394–407.
[22] P.A. Jackson, J.C. Widen, D.A. Harki, K.M. Brummond, Covalent Modifiers: A chemical perspective on the reactivity of α, β-unsaturated carbonyls with thiols *via* hetero-michael addition reactions, J. Med. Chem. 60 (2017) 839–885.
[23] J. Yang, Y. Wang, T. Wang, J. Jiang, H.C. Botting, H. Liu, Q. Chen, J. Yang, J.H. Naismith, X. Zhu, L. Chen, Pironetin reacts covalently with cysteine-316 of α-tubulin to destabilize microtubule, Nat. Commun. 7 (2016) 12103.
[24] T.Y. Chang, Y.P. Tu, W.Y. Wei, H.Y. Chen, C.S. Chen, Y.S.E. Lee, J.J. Huang, C.K. Sha, Synthesis and Antiproliferative Activities of Ottelione A Analogues, ACS Med. Chem. Lett. 3 (2012) 1075–1080.
[25] a) R. Bai, C. Duanmu, E. Hamel, Mechanism of action of the antimitotic drug 2,4-dichlorobenzyl thiocyanate: alkylation of sulfhydryl group(s) of β-tubulin, Biochim Biophys Acta 994 (1989) 12–20;
b) B. Shan, J.C. Medina, E. Santha, W.P. Frankmoelle, T. Chou, R.M. Learned, M.R. Narbut, D. Stott, P. Wu, J.C. Jaen, T. Rosen, P.B.M.W.M. Timmermans, H. Beckmann, Selective, covalent modification of β-tubulin residue Cys-239 by T138067, an antitumor agent with in vivo efficacy against multidrug-resistant

tumors, Proc. Natl. Acad. Sci. USA 96 (1999) 5686–5691;
c) Y. Lu, J. Chen, J. Wang, C. Li, S. Ahn, C.M. Barrett, J.T. Dalton, W. Li, D.D. Miller, Design synthesis and biological evaluation of stable colchicine binding site tubulin inhibitors as potential anticancer agents, J. Med. Chem. 57 (2014) 7355–7366;
d) R. Bai, D.G. Covell, X.F. Pei, J.B. Ewell, N.Y. Nguyen, A. Brossi, E. Hamel, Mapping the binding site of colchicinoids on beta -tubulin. 2-Chloroacetyl-2-demethylthiocolchicine covalently reacts predominantly with cysteine 239 and secondarily with cysteine 354, J Biol Chem 275 (2000) 40443–40452.

[26] a) N.P. Kumar, P. Sharma, T.S. Reddy, N. Shankaraiah, S.K. Bhargava, A. Kamal, Microwave-assisted one-pot synthesis of new phenanthrene fused tetrahydrodibenzo-acridinones as potential cytotoxic and apoptosis inducing agents, Eur. J. Med. Chem. 151 (2018) 173–185;
b) C.S. Digwal, U. Yadav, P.V.S. Ramya, S. Sana, B. Swain, A. Kamal, Vanadium-catalyzed oxidative C(CO)–C(CO) bond cleavage for C-N bond formation: one-pot domino transformation of 1,2-diketones and amidines into imides and amides, J. Org. Chem. 82 (2017) 7332–7345.

[27] a) N.P. Kumar, P. Sharma, T.S. Reddy, S. Nekkanti, N. Shankaraiah, G. Lalita, S.S. Kumara, S.K. Bhargava, V.G.M. Naidu, A. Kamal, Synthesis of 2,3,6,7-tetramethoxy phenanthren-9-amine: An efficient precursor to access new 4-aza-2,3-dihydropyrido phenanthrenes as apoptosis inducing agents, Eur. J. Med. Chem. 127 (2017) 305–317;
b) P. Sharma, K.R. Senwar, M.K. Jeengar, T.S. Reddy, V.G.M. Naidu, A. Kamal, N. Shankaraiah, H2O-Mediated isatin spiro-epoxide ring opening with NaCN: Synthesis of novel 3-tetrazolylmethyl-3-hydroxy-oxindole hybrids and their anticancer evaluation, Eur. J. Med. Chem. 104 (2015) 11–24;
c) S. Nekkanti, V. Pooladanda, M. Veldandi, R. Tokala, C. Godugu, N. Shankaraiah, Synthesis of 1,2,3-triazolo-fused-tetrahydro-β-carboline derivatives via 1,3-dipolar cycloaddition reaction: Cytotoxicity evaluation and DNA-binding studies, ChemistrySelect 2 (2017) 7210–7221;
d) R. Tokala, S. Thatikonda, S. Sana, P. Regur, C. Godugu, N. Shankaraiah, Synthesis and in vitro cytotoxicity evaluation of β-carboline-linked 2,4-thiazolidinedione hybrids: Potential DNA intercalation and apoptosis inducing studies, New J. Chem. 42 (2018) 16226–16236.

[28] a) A.S. Mostafa, K.B. Selim, Synthesis and anticancer activity of new dihydropyrimidinone derivatives, Eur. J. Med. Chem. 156 (2018) 304–315;
b) A. Crespo, A. El, P. Maatougui, J. Biagini, A. Azuaje, J. Coelho, M.I. Brea, M.I. Loza, X. Cadavid, H. García-Mera, E. Sotelo Gutiérrez-de-Terán, Discovery of 3,4-dihydropyrimidin-2(1H)-ones as a novel class of potent and selective A2B Adenosine Receptor Antagonists, ACS Med. Chem. Lett. 4 (2013) 1031–1036.

[29] N.P. Kumar, S. Thatikonda, R. Tokala, S.S. Kumari, U.J. Lakshmi, C. Godugu, N. Shankaraiah, A. Kamal, Sulfamic acid promoted one-pot synthesis of phenanthrene fused-dihydrodibenzo-quinolinones: Anticancer activity, tubulin polymerization inhibition and apoptosis inducing studies, Bioorg. Med. Chem. 26 (2018) 1996–2008.

[30] N. Shankaraiah, S. Nekkanti, U.R. Brahma, N.P. Kumar, N. Deshpande, D. Prasanna, K.R. Senwar, U.J. Lakshmi, Synthesis of different heterocycles-linked chalcone conjugates as cytotoxic agents and tubulin polymerization inhibitors, Bioorg. Med. Chem. 25 (2017) 4805–4816.

[31] a) K.T. Chan, F.Y. Meng, Q. Li, C.Y. Ho, T.S. Lam, Y. To, W.H. Lee, M. Li, K.H. Chu, M. Toh, Cucurbitacin B induces apoptosis and S phase cell cycle arrest in BEL-7402 human hepatocellular carcinoma cells and is effective via oral administration, Cancer Lett. 294 (2010) 118–124;
b) J.K. Shen, H.P. Du, M. Yang, Y.G. Wang, J. Jin, Casticin induces leukemic cell death through apoptosis and mitotic catastrophe, Ann. Hematol. 88 (2009) 743–752.

[32] a) B.I. Tarnowski, F.G. Spinale, J.H. Nicholson, DAPI as a useful stain for nuclear quantitation, Biotech Histochem. 66 (1991) 297–302;
b) L. Li, L. Dong, J. Zhang, F. Gao, J. Hui, J. Yan, Mesenchymal stem cells with downregulated Hippo signaling attenuate lung injury in mice with lipopolysaccharide-induced acute respiratory distress syndrome, Int J Mol Med. 43 (2019) 1241–1252;
c) R. Tokala, S. Thatikonda, U.S. Vanteddu, S. Sana, C. Godugu, N. Shankaraiah, Design and synthesis of DNA-interactive β-carboline-oxindole hybrids as cytotoxic and apoptosis inducing agents, ChemMedChem 13 (2018) 1909–1922.

[33] a) K. Liu, P. Liu, R. Liu, Dual AO/EB Staining to Detect Apoptosis in Osteosarcoma Cells Compared with Flow Cytometry, Med Sci Monit Basic Res. 21 (2015) 15–20;
b) N.P. Kumar, S. Nekkanti, S.S. Kumari, P. Sharma, N. Shankaraiah, Design and synthesis of 1,2,3-triazolo-phenanthrene hybrids as cytotoxic agents, Bioorg. Med. Chem. Lett 27 (2017) 2369–2376.

[34] M. Mirsaeidi, S. Gidfar, A. Vu, D. Schraufnagel, Annexins family: insights into their functions and potential role in pathogenesis of sarcoidosis, J Transl Med. 14 (2016) 89.

[35] A. Kamal, T.S. Reddy, M.V.P.S. Vishnuvardhan, V.D. Nimbarte, A.V. Subba Rao, V. Srinivasulu, N. Shankaraiah, Synthesis of 2-aryl-1,2,4-oxadiazolo-benzimidazoles: Tubulin polymerization inhibitors and apoptosis inducing agents, Bioorg. Med. Chem. 23 (2015) 4608–4623.

[36] E. Eruslanov, S. Kusmartsev, Identification of ROS using oxidized DCFDA and flow-cytometry, Methods. Mol. Biol. 594 (2010) 57–72.

[37] R. Tokala, S. Bale, I.P. Janrao, A. Vennela, N.P. Kumar, K.R. Senwar, C. Godugu, N. Shankaraiah, Synthesis of 1,2,4-triazole-linked urea/thiourea conjugates as cytotoxic and apoptosis inducing agents, Bioorg. Med. Chem. Lett. 28 (2018) 1919–1924.

[38] A.M. Rieger, K.L. Nelson, J.D. Konowalchuk, D.R. Barreda, Modified annexin V/propidium iodide apoptosis assay for accurate assessment of cell death, J Vis Exp. 50 (2011) 2597.

[39] C.P. LeBel, H. Ischiropoulos, S.C. Bondy, Evaluation of the probe 2',7'-dichlorofluorescin as an indicator of reactive oxygen species formation and oxidative stress, Chem. Res. Toxicol. 5 (1992) 227–231.